Evolution of a biochemical model of steady-state photosynthesis

Yin, Xinyou; Busch, Florian A.; Struik, Paul C.; Sharkey, Thomas D.

DOI:
10.1111/pce.14070

Document Version
Peer reviewed version

Citation for published version (Harvard):
Yin, X, Busch, FA, Struik, PC & Sharkey, TD 2021, 'Evolution of a biochemical model of steady-state photosynthesis', *Plant, Cell and Environment*, vol. 44, no. 9, pp. 2811-2837. https://doi.org/10.1111/pce.14070

Evolution of a biochemical model of steady-state photosynthesis

Xinyou Yin[1,*], Florian A. Busch[2], Paul C. Struik[1], and Thomas D. Sharkey[3]

[1] Centre for Crop Systems Analysis, Wageningen University & Research, P.O. Box 430, 6700 AK Wageningen, The Netherlands

[2] School of Biosciences and Birmingham Institute of Forest Research, University of Birmingham, Birmingham, B15 2TT, United Kingdom

[3] MSU-DOE Plant Research Laboratory, Plant Resilience Institute, Michigan State University, 612 Wilson Rd, East Lansing, MI 48824, USA

(*For correspondence: Xinyou.yin@wur.nl)

Running title: Evolution of a biochemical model of photosynthesis

Abstract

On the occasion of the 40th anniversary of the publication of the landmark model by Farquhar, von Caemmerer & Berry on steady-state C_3 photosynthesis (known as the "FvCB model"), we review three major further developments of the model. These include: (1) limitation by triose phosphate utilisation, (2) alternative electron transport pathways, and (3) photorespiration-associated nitrogen and C_1 metabolisms. We discussed the relation of the third extension with the two other extensions, and some equivalent extensions to model C_4 photosynthesis. In addition, the FvCB model has been coupled with CO_2-diffusion models. We review how these extensions and integration have broadened the use of the FvCB model in understanding photosynthesis, especially with regard to bioenergetic stoichiometries associated with photosynthetic quantum yields. Based on the new insights, we present caveats in applying the FvCB model. Further research needs are highlighted.

Keywords: (alternative) electron transport, mesophyll conductance, NADPH-ATP balance, nitrogen assimilation, photorespiration, quantum yield, re-assimilation, stoichiometry, triose phosphate utilisation.

Introduction

The year of writing this paper marks the 40th anniversary of the widely used biochemical model of Farquhar, von Caemmerer & Berry (1980) on C_3 photosynthesis, known as the "FvCB model" (see Table 1 for all acronyms). The model is a mathematical representation of the biochemical processes in the chloroplast related to photosynthetic CO_2 uptake of plants. The application of this model has gone far beyond the developers' expectations even 20 years ago (see the reflections by Farquhar et al. 2001) and continues to rapidly rise today. It has become one of the most widely used models in plant science and beyond. For understanding leaf physiology, the model has been used to analyse gas exchange (sometimes combined with chlorophyll fluorescence) data (e.g. von Caemmerer & Farquhar 1981; Long & Bernacchi 2003; Sharkey et al. 2007; Yin et al. 2009), to understand photosynthetic control of electron transport (e.g. Foyer et al. 2012), and to quantify photosynthetic limitations (e.g. Busch & Sage 2017; Deans et al. 2019). When coupled to models of stomatal control it contributes to understanding how water is traded for CO_2 (Farquhar & Wong, 1984; Leuning, 1990) and how photosynthetic gas-exchange and water-relation traits are coordinated (Deans et al. 2020). The FvCB model forms the basis of our understanding of photosynthetic isotope discrimination (Farquhar et al. 1982; Farquhar 1983; Ubierna et al. 2019; Busch et al. 2020). It has also been used to scale photosynthetic processes from the chloroplast and leaf level to higher levels (Yin & Struik 2008; Bagley et al. 2015; Wu et al. 2019), for assessing the impact of genetic engineering for identified photosynthetic targets on canopy productivity (e.g. Zhu et al. 2004) and crop yield (Yin & Struik 2017a). The model is even used to inform

climate models (Pitman 2003) and describe plant carbon uptake on the global level as a component of Earth System Models (Sellers et al. 1996; Rogers et al. 2014). Here we take a historical view of the original FvCB model and subsequently go into details of how this model has been extended since then.

The FvCB model represents a simplified view of the then available knowledge of major mechanisms, especially on the finding that O_2 is an alternative substrate of Rubisco, leading to photorespiration. The model describes the net rate of CO_2-assimilation (A; see Table 2 for definitions of all model symbols) as the difference between carboxylation rate (V_c) and loss through photorespiration (a consequence of the oxygenation rate; V_o) and respiratory activities other than photorespiration, called "day respiration" (R_d). Assuming the photorespiratory pathway is a closed cycle, 0.5 mol CO_2 is released when Rubisco catalyses the reaction with one mol O_2 (see discussion later) such that A is expressed as:

$$A = V_c - 0.5V_o - R_d = (1 - 0.5\phi)V_c - R_d \quad (1)$$

where ϕ is the oxygenation to carboxylation ratio. R_d has also been called "mitochondrial respiration in the light", but the term "day respiration" is preferred. This is to remain non-specific about where the respired CO_2 comes from, as CO_2 released is not necessarily mitochondrial in origin (Tcherkez et al. 2017). The model ignores any possible consumption of chloroplastic NADPH or ATP if R_d does not originate in mitochondria.

The photosynthetic carbon-reduction cycle, the Calvin-Benson cycle, starts with the carboxylation of the CO_2 acceptor ribulose 1,5-bisphosphate (RuBP), a five-carbon molecule. The reaction is catalysed by Rubisco, yielding two mol of the three-carbon molecule 3-phosphoglycerate (3-PGA) for every mol RuBP carboxylated. When CO_2 supply is limiting (or when RuBP is saturating), V_c is limited by RuBP-saturated Rubisco kinetics and can be described as W_c by the Michaelis-Menten equation appropriate for the case where two substrates (CO_2 and O_2) compete for active sites of RuBP-bound Rubisco:

$$V_c = W_c = \frac{C_c V_{cmax}}{C_c + K_{mC}(1 + O_c/K_{mO})} \quad (2a)$$

Likewise, V_o can be expressed as:

$$V_o = \frac{O_c V_{omax}}{O_c + K_{mO}(1 + C_c/K_{mC})} \quad (2b)$$

where C_c and O_c are the level of CO_2 and O_2 at the active sites of Rubisco, respectively; V_{cmax} and V_{omax} are the maximum rate of carboxylation and oxygenation of Rubisco, respectively; and K_{mC} and K_{mO} are the Michaelis-Menten constants of Rubisco for CO_2 and O_2, respectively. One can derive the expression for the V_c : V_o ratio from combining eqn 2a and eqn 2b as: $[V_{cmax}K_{mO}/(V_{omax}K_{mC})]C_c/O_c$, where the whole term within the [ ] has been defined as the relative CO_2/O_2 specificity of Rubisco, $S_{c/o}$ (Laing et al. 1974). If we use Γ_* to denote the CO_2 level at which the rate of CO_2 uptake by carboxylation is balanced by the rate of photorespiratory CO_2 release (i.e., $V_c = 0.5V_o$), also called the CO_2-compensation point in the absence of day respiration, Γ_* can be expressed as $0.5O_c/S_{c/o}$ (Farquhar et al. 1980). Furthermore, the V_o : V_c ratio, or ϕ can be expressed thereof as $2\Gamma_*/C_c$ (Farquhar et al. 1980). Therefore, eqn 1 can be written as: $A = (1 - \Gamma_*/C_c)V_c - R_d$.

Photosynthesis can also depend on the rate at which RuBP is regenerated. This usually occurs at high CO_2 concentration and/or low light. The model assumes RuBP regeneration-limited photosynthesis is controlled by electron transport (Farquhar et al. 1980). Photosynthetic linear electron transport (LET) produces both NADPH and ATP; so, RuBP regeneration-limited or electron transport-limited carboxylation rate, W_j, can be formulated in terms of either NADPH supply or ATP supply from LET:

NADPH supply: $$W_j = \frac{(1/2)J}{2 + 2\phi} = \frac{C_c J}{4C_c + 8\Gamma_*} \quad (3a)$$

ATP supply: $$W_j = \frac{(2/3)J}{3 + 3.5\phi} = \frac{C_c J}{4.5C_c + 10.5\Gamma_*} \quad (3b)$$

where J is the rate of potential LET.

Eqn 3a is based on the stoichiometry of NADPH or electron requirement by the Calvin-Benson cycle and the photorespiratory cycle. First, carboxylation of one mol RuBP results in two mol 3-PGA, reduction of each 3-PGA to triose phosphate (TP) requires one mol NADPH (Fig. 1a), and production of one mol NADPH requires two mol electrons; so, four electrons are required per carboxylation. The whole term in the numerator, (1/2)*J*, represents the rate of NADPH production from LET. Secondly, although oxygenation of one mol RuBP initially results in only one mol 3-PGA, it also results in one mol of the two-carbon molecule, 2-phosphoglycolate, which is dephosphorylated to glycolate in the chloroplast (Fig. 1a,b). The glycolate is transported from the chloroplast into the peroxisome, where it is converted to glyoxylate and further to glycine (two carbons). The glycine is exported to the mitochondrion, where 0.5 mol glycine and tetrahydrofolate (THF) are converted by glycine decarboxylase (GDC) to 5,10-methylene-tetrahydrofolate (CH_2-THF), releasing 0.5 mol ammonia and 0.5 mol CO_2 in the process. CH_2-THF reacts with the remaining 0.5 mol glycine to form 0.5 mol serine (three carbons). Serine moves to the peroxisome and is transformed to glycerate. The glycerate flows to the chloroplast and is converted to 0.5 mol 3-PGA. Its reduction before incorporation into the Calvin-Benson cycle consumes 0.5 mol NADPH. The 0.5 mol ammonia released by GDC is re-assimilated into glutamate requiring one mol reduced ferredoxin (equivalent to 0.5 mol NADPH). In sum, the photorespiratory cycle involving three organelles (chloroplast, peroxisome, and mitochondrion, Fig. 1b) requires four electrons per oxygenation.

In eqn 3b, the coefficient 2/3 stems from understandings of that time (in 1980) about the stoichiometry that each mol electron in LET translocates two mol protons (H^+) across the thylakoid membrane into the lumen, and synthesis of one mol ATP requires three mol H^+; so, the whole term in the numerator, (2/3)*J*, represents the rate of ATP production from LET. The coefficient 3 in the denominator refers to the requirement of three mol ATP per mol RuBP

carboxylated by the Calvin-Benson cycle, consisting of two mol ATP for the phosphorylation of two mol 3-PGA to two mol 1,3-bisphosphoglycerate (before the reduction step consuming NADPH) and one mol ATP for the subsequent phosphorylation of one mol ribulose 5-phosphate to one mol RuBP (Fig. 1a). The coefficient 3.5 refers to the ATP requirement per oxygenation by the photorespiratory cycle. This consists of: (1) one mol ATP for the phosphorylation of one mol 3-PGA to one mol 1,3-bisphosphoglycerate before its reduction, (2) one mol ATP for the phosphorylation of ribulose 5-phosphate to RuBP, (3) 0.5 mol ATP for the phosphorylation of glycerate to 3-PGA plus 0.5 mol ATP for the subsequent phosphorylation of this 0.5 mol 3-PGA, and (4) 0.5 mol ATP for the re-assimilation of 0.5 mol ammonia (Fig. 1a).

There are several equation forms describing J in eqn 3a and eqn 3b as a function of absorbed irradiance (I_{abs}), but a non-rectangular hyperbolic function as the smaller root to the quadratic equation of Farquhar & Wong (1984) is mostly used now:

$$J = \frac{0.5(1-f)I_{abs}+J_{max}-\sqrt{[0.5(1-f)I_{abs}+J_{max}]^2-4\theta[0.5(1-f)]I_{abs}J_{max}}}{2\theta} \quad (4)$$

where J_{max} is the maximum rate of LET under the saturating irradiance, f is the fraction of I_{abs} unavailable for Calvin-Benson and photorespiratory cycles, 0.5 refers to the partitioning factor of the light energy between the two photosystems, and θ is the curvature factor.

The carboxylation rate can be limited either by RuBP-saturated rate W_c or by RuBP-regeneration determined rate W_j; so, eqn 1 becomes:

$$A = (1-0.5\phi)\min(W_c, W_j) - R_d = \left(1-\frac{\Gamma_*}{C_c}\right)\min(W_c, W_j) - R_d \quad (5)$$

Eqn 5, combined with eqn 2a for W_c, eqn 3a or 3b for W_j and eqn 4 for J, forms the basic FvCB model. We shall call it the canonical FvCB model.

Since its first publication, the model has been developed further several times for C_3 photosynthesis (Sharkey 1985a,b; Harley & Sharkey 1991; Yin et al. 2004; Busch et al. 2018; Busch 2020) and extended for C_4 photosynthesis (von Caemmerer & Furbank 1999). Also,

this model has been integrated with models for mesophyll CO_2-diffusion for various applications. In this paper, we outline the major extensions and review how these extensions and integration have broadened the use of the model in exploring the underlying physiology of photosynthesis.

Extension 1: Introducing the third limitation set by triose phosphate utilisation

Accommodating photosynthetic insensitivity to CO_2 and O_2

The canonical FvCB model predicts that A will always increase with increasing CO_2 level, despite a lower increase in the W_j-limited range than in the W_c-limited range. However, many (e.g. Sharkey 1985a) showed that A can be insensitive to changes in the CO_2 partial pressure within the high CO_2 range, in particular in combination with high irradiance, or low O_2 partial pressure, or at low temperature. Sharkey (1985b) hypothesised that this insensitivity was due to the limitation set by the rate at which TP are utilised in the synthesis of sucrose or starch. As the use of TP is stoichiometrically exchanged with the release of phosphate (P_i) during sucrose or starch synthesis, a limitation in TP utilisation (TPU) could result in a limitation to photophosphorylation, and, thus, to RuBP regeneration. So, in addition to what has been assumed about the control of RuBP regeneration by electron transport in the canonical FvCB model, RuBP regeneration can be limited further by other components as in the Calvin-Benson cycle and beyond. If TPU limits, the equation for A, equivalent to eqn 5, in the FvCB model, should be extended as:

$$A = (1 - 0.5\phi)\min(W_c, W_j, W_p) - R_d = \left(1 - \frac{\Gamma_*}{C_c}\right)\min(W_c, W_j, W_p) - R_d \qquad (6a)$$

where W_p is the rate of carboxylation set by TPU limitation.

The carboxylation of one mol RuBP results in two mol TP but the Calvin-Benson cycle stoichiometry suggests that only one-sixth of the TP is used for sucrose or starch synthesis

whereas the remaining five-sixths of the TP are drawn back into the cycle to contribute to the regeneration of RuBP (Taiz & Zeiger 2002). Thus, the P_i consumption by sucrose or starch synthesis is $2V_c/6 = V_c/3$. Considering the carbon loss in the photorespiratory cycle, the net P_i consumption would be $(1-0.5\phi)V_c/3$, and this must be equal to the release of P_i via TPU if P_i is limiting. Let T_p be the rate of TPU, then one can write:

$$V_c = W_p = \frac{T_p}{(1-0.5\phi)/3} = \frac{C_c(3T_p)}{C_c-\Gamma_*} \quad (6b)$$

Substituting eqn 6b into eqn 6a gives the net CO_2-assimilation rate limited by TPU, A_p, as:

$$A_p = 3T_p - R_d \quad (6c)$$

This is the simple equation given first by Sharkey (1985b), which suggests that if TPU is limiting, A is no longer sensitive to changes in CO_2 or O_2 partial pressure, or in irradiance. It sets an upper limit to net assimilation rate.

Accommodating the reversed sensitivity to CO_2 and O_2

It has been frequently observed that A even declines with increasing CO_2 partial pressure within the high CO_2 range, particularly under low O_2 conditions (e.g. von Caemmerer & Farquhar 1981). Similarly, increasing O_2 has been observed to stimulate CO_2 assimilation under high CO_2 conditions (Harley & Sharkey (1991). These reversed sensitivities to CO_2 and O_2 cannot be explained by the simple model, eqn 6c.

Sharkey & Vassey (1989) proposed that the reverse sensitivity was caused by inhibition of starch synthesis capacity, and in turn caused reduced stromal phosphoglucoisomerase activity resulting from metabolites interfering with its activity. An alternative explanation was proposed by Harley & Sharkey (1991) that a fraction of the glycolate carbon, which leaves the chloroplast and is recycled to glycerate in the photorespiratory cycle, does not return to the chloroplast, but after converting to glycine, is diverted from the photorespiratory cycle and used elsewhere for amino acid synthesis. Thus, the P_i normally used in converting glycerate to

3-PGA is made available for phosphorylation instead, thereby, stimulating RuBP regeneration. Based on this hypothesis, Harley & Sharkey (1991) used three values for the fraction (0.0, 0.5, and 1.0) to fit data and showed how the curvature of photosynthetic CO_2-response curves (A-C_i curves) had varying extents of the reversed CO_2 and O_2 sensitivity.

Based on the analysis by Harley & Sharkey (1991), von Caemmerer (2000) formalised the model by using α as the fraction of the glycolate carbon that is not returned to the chloroplast. As one oxygenation produces 0.5 glycerate, which consumes one P_i, the rate of P_i consumption, which usually is $(1-0.5\phi)V_c/3$, should be decreased by $\alpha V_o/2$, or $\alpha\phi V_c/2$. Thus, the net P_i consumption in this case would be $[(1-0.5\phi)/3-\alpha\phi/2]V_c$. In analogy to eqn 6b, W_p as the rate of carboxylation set by TPU limitation becomes:

$$W_p = \frac{T_p}{(1-0.5\phi)/3-\alpha\phi/2} = \frac{3T_p}{1-0.5\phi(1+3\alpha)} = \frac{C_c(3T_p)}{C_c-(1+3\alpha)\Gamma_*} \quad (7a)$$

The model for the net CO_2-assimilation rate, A_p, becomes:

$$A_p = \frac{(C_c-\Gamma_*)(3T_p)}{C_c-(1+3\alpha)\Gamma_*} - R_d \quad (7b)$$

where $0 \le \alpha \le 1$. If $\alpha = 0$, eqn 7b becomes eqn 6c, representing the case that glycolate carbon maximally returns to the chloroplast (i.e. ¾ of the glycolate carbon is recycled as glycerate; the other ¼ is lost as CO_2 as the result of glycine decarboxylation). Harley & Sharkey (1991) showed that for the same value of α, TPU starts to limit A at a lowering CO_2 level with increasing irradiance, with decreasing O_2 level, and with decreasing temperature. The reverse sensitivity that can occur based on eqn 7b is frequently observed but occasionally the reverse sensitivity is greater than what can be accounted for by eqn 7b. It is likely that both the incomplete photorespiratory cycle explanation and the starch inhibition explanation (Sharkey & Vassey 1989) can be valid, although in our experience the incomplete photorespiratory cycle phenomenon is more common.

Implications of TPU limitation in modelling leaf photosynthesis

Ellsworth et al. (2015) showed that TPU limitations to photosynthetic capacity are common in woody species grown in the field. However, TPU might not be the most important limitation under current climatic growth conditions, as evidenced by Kumarathunge et al. (2019), who reported that only *ca* 30% of A-C_i curves showed an obvious TPU limitation in a global data representing 141 species. Irrespective of its uncertain importance under field conditions, the inclusion of TPU limitation in models is important for elucidating the basic principles of photosynthetic mechanisms. In cases where TPU is actually limiting, the canonical, two-limitation FvCB model would underestimate J_{max} (when fitting to A-C_i curves) and V_{cmax} or J_{max} (when fitting to light response curves) because the maximum photosynthetic rate would be wrongly attributed to being limited by electron transport or by Rubisco activity.

It is important to note that TPU limitation is a form of very short-term sink : source disequilibrium (McClain & Sharkey (2019). It concerns the ability to remove TP quickly from the Calvin-Benson cycle. The half-life time of the cycle intermediates can be shorter than 1 s, while some larger pools still have a half-life time of < 1 min. This means that TPU limitation can build up and disappear quickly. As discussed by Sharkey (2019), when plants are put into TPU limited conditions for hours or days, the TPU limitation is observable at first; but then other components like electron transport are regulated to a level that TPU is no longer "apparently" limiting (e.g. Pammenter et al. 1993). Furthermore, over a longer time, a larger sink can remove short-term TPU limitation. Kaschuk et al. (2012) showed that nodulated soybean plants had 14-31% higher rates of photosynthesis and accumulated less starch in the leaves than nitrogen-fertilized plants, supporting that rhizobial symbiosis could stimulate photosynthesis due to the removal of carbon sink limitation by nodule activities.

Conversely, a small sink, especially when combined with a large source, can cause TPU limitation. Fabre et al. (2019) reported the occurrence of TPU limitation in panicle-pruned

rice plants, especially those grown under 800 μmol mol^{-1} CO_2. This reduction was associated with sucrose accumulation in the flag leaf resulting from the sink limitation. The photosynthetic stimulation by the elevated-CO_2 was lower in pruned plants compared with control plants, and this response to CO_2 in relation to sink size was also found when comparing various rice genotypes having contrasting leaf : panicle size ratios or source : sink ratios (Fabre et al. 2020). A recent review by Dingkuhn et al. (2020) even found the evidence from broader ranges of genotypes that stronger elevated-CO_2 responsiveness in wild relatives and old cultivars of crops is related to sink strength as a result of adaptive plasticity involving branching. Perhaps the most important result in recent work of Fabre et al. is that TPU, thus net CO_2 assimilation rate, declines increasingly with time after the midday in a diurnal cycle. These findings suggest that not only TPU limitation in regulating photosynthesis should be considered, but also a shorter time-step would be needed to account for diurnal variations in sink feedback limitation to photosynthesis, in dynamic crop models for projecting the CO_2-fertilisation effect on crop production.

Extension 2: Introducing alternative electron transport pathways

Accommodating a balanced ATP:NADPH ratio

In the canonical FvCB model, there are two different equations, eqn 3a and eqn 3b, for the same electron transport-limited carboxylation rate, W_j. By comparison of the two equations, one can immediately recognise that the value of W_j determined by the ATP supply is more limiting than that determined by the NADPH supply. The two equations were used largely in a random manner in the literature before 2000. To eliminate the "random" application of the FvCB model, Yin et al. (2004) developed a generalised model that covers, among others, the two forms of the FvCB model for the electron transport-limited rate.

It is apparent that, according to the stoichiometric coefficients accepted in 1980, the LET produces an ATP:NADPH ratio of 1.333 [resulting from (2/3):(1/2), see eqn 3a vs 3b], well below 1.5 as required by the Calvin-Benson cycle, with ATP in deficit relative to NADPH. Chloroplasts engage several mechanisms that could remove the disparity in terms of requirement for the correct ATP:NADPH ratio (Farquhar & von Caemmerer 1982; Allen 2003; Baker et al. 2007). First, instead of going to the end electron acceptor $NADP^+$, a fraction of electrons passing PSI may follow a cyclic electron pathway (f_{cyc}) (Fig. 2). The cyclic electron transport (CET) does not produce NADPH, but passes through the "coupling" sites of ATP synthase (Allen 2003), thereby being able to increase the ATP:NADPH ratio. Second, part of the noncyclic electrons may be used to support processes like the Mehler ascorbate peroxidase reaction or nitrate reduction, where O_2 directly or nitrate indirectly act as the electron acceptors, respectively (Fig. 2). Every one mol O_2 uptake in the Mehler ascorbate peroxidase reaction is accompanied by one mol O_2 production from the splitting of water at PSII; so this reaction consumes four electrons per O_2 but requires no ATP (Asada 1999). The first step of the reduction of nitrate into nitrite takes place in the cytosol but may use reducing power generated in the chloroplast (e.g. via the malate shuttle) and the subsequent steps in converting nitrite to ammonia and to glutamate take place in the chloroplast stroma, using the reduced ferredoxin (Noctor & Foyer 1998). One mol nitrate reduction requires 10 mol electrons and only one mol ATP (Noctor & Foyer 1998). Thus, both the Mehler ascorbate peroxidase reaction and nitrate reduction can help to adjust the ATP:NADPH ratio as required by the Calvin-Benson and the photorespiratory cycles. There are some other minor processes like sulphur assimilation and fatty acid biosynthesis that might use chloroplastic electrons but these are quantitatively less significant. For the convenience of modelling, the noncyclic electron transport in support of the Mehler ascorbate peroxidase reaction, nitrate reduction and any other minor processes is collectively named as the pseudocyclic category, and this

fraction is denoted as f_{pseudo} (Yin et al. 2004). Therefore, the fraction for LET (i.e. the fraction of the total electron flux passing PSI that is to support the Calvin-Benson and the photorespiratory cycles) is $(1-f_{cyc}-f_{pseudo})$ (Fig. 2). Yin et al. (2004) derive a relationship for fractions of various electron transport pathways that must be met in order to ensure that the produced ATP:NADPH ratio is compatible with the required ratio by the Calvin-Benson and the photorespiratory cycles:

$$1 - f_{\mathrm{cyc}} - f_{\mathrm{pseudo}} = \frac{(4C_{\mathrm{c}}+8\Gamma_*)(2+f_{\mathrm{Q}}-f_{\mathrm{cyc}})}{h(3C_{\mathrm{c}}+7\Gamma_*)} \quad (8)$$

where h is the number of H^+ required per ATP synthesis and f_Q is the fraction of electrons at the plastoquinone that follows the Q cycle (Fig. 2).

In the presence of CET, the PSI electron flux (J_1) is higher than the PSII electron flux (J_2): $J_1 = J_2/(1-f_{cyc})$ (Yin et al. 2004). The LET in support of the Calvin-Benson and the photorespiratory cycle is $(1-f_{cyc}-f_{pseudo})J_1$ (Fig. 2). Combining these equations with eqn 3a of the FvCB model gives:

$$\text{NADPH supply: } W_{\mathrm{j}} = \left(1 - f_{\mathrm{cyc}} - f_{\mathrm{pseudo}}\right)\frac{C_{\mathrm{c}}J_1}{4C_{\mathrm{c}}+8\Gamma_*} = \left(1 - \frac{f_{\mathrm{pseudo}}}{1-f_{\mathrm{cyc}}}\right)\frac{C_{\mathrm{c}}J_2}{4C_{\mathrm{c}}+8\Gamma_*} \quad (9a)$$

Substituting eqn 8 to eqn 9a gives:

$$\text{ATP supply:} \qquad W_{\mathrm{j}} = \frac{(2+f_{\mathrm{Q}}-f_{\mathrm{cyc}})C_{\mathrm{c}}J_2}{h(1-f_{\mathrm{cyc}})(3C_{\mathrm{c}}+7\Gamma_*)} \quad (9b)$$

The two forms of electron transport-limited part of the canonical FvCB model are special cases of this extended model. If $f_{pseudo} = 0$, eqn 9a becomes eqn 3a; in such a case, the whole PSII electron flux equals the LET ($J_2 = J$). If $f_Q = 0$, $h = 3$, and $f_{cyc} = 0$, eqn 9b becomes eqn 3b. So, the canonical FvCB model implies no operation of the Q cycle and a requirement of three H^+ per ATP synthesis (the H^+:ATP ratio $h = 3$).

However, the contemporary belief is that the Q cycle may operate obligatorily ($f_Q = 1$; e.g. Sacksteder et al. 2000), and this cycle will effectively double the stoichiometry of the H^+ translocation through the cytochrome b_6f complex from one H^+ to two H^+ per electron passed

1 therein (Fig. 2). So, plus one H^+ pumped from splitting the water molecule through the PSII
2 complex, a total of three H^+ (instead of two) produced per electron are transferred along the
3 whole-chain if the Q cycle operates (von Caemmerer 2000; also see Fig. 2). Also, the H^+:ATP
4 ratio is probably either 4 based on thermodynamic experiments (Steigmiller et al. 2008;
5 Peterson et al. 2012) or 4.67 (=14/3) from the structural data for the c14 rotor ring of the H^+
6 translocating chloroplast ATP synthase (Seelert et al. 2000; Hahn et al. 2018), instead of 3
7 used in the FvCB model. If $f_Q = 1$, $h = 4$, and $f_{cyc} = 0$, then the produced ATP:NADPH ratio
8 from the noncyclic electron pathway is 1.5, exactly matching the ratio required by the Calvin-
9 Benson cycle and eqn 9b becomes eqn 2.22 of von Caemmerer (2000) for this scenario, i.e.,

10 $$W_j = \frac{C_c J}{4C_c + 9.33\Gamma_*} \quad (9c)$$

11 If $f_Q = 1$, $h = 4.67$, and $f_{cyc} = 0$, the ATP:NADPH ratio from the noncyclic electron pathway is
12 1.286 (even lower than 1.333 assumed in the canonical FvCB model), and the value has often
13 been cited in the recent literature to stress the surplus of the reducing power which might be
14 exported to cytosol (e.g. Lim et al. 2020). For such a case, eqn 9b becomes:

15 $$W_j = \frac{C_c J}{4.67C_c + 10.89\Gamma_*} \quad (9d)$$

16 Clearly, the model of Extension 2 represents the generalised algorithm for various scenarios
17 with regard to the H^+:electron and the H^+:ATP ratios. Eqn 9b actually contains the ATP
18 production factor (z) per electron transferred through PSII when CET occurs simultaneously
19 (also see eqn B8b in their Appendix B of Yin et al. 2004):

20 $$z = \frac{2 + f_Q - f_{cyc}}{h(1 - f_{cyc})} \quad (9e)$$

21 This ATP:electron ratio factor z is 2/3 in eqn 3b of the canonical FvCB model, 3/4 in the case
22 of eqn 9c, and 9/14 in the case of eqn 9d. The z factor also predicts that for a given set of f_Q
23 and h, the ATP:electron ratio increases expectedly with increasing f_{cyc}. Given that the Q cycle
24 may not necessarily switch absolutely on ($f_Q = 1$) and off ($f_Q = 0$) but run partially (Cornic et

al. 2000), the model allows such scenarios with $0 \leq f_Q \leq 1$. As noted by Yin et al. (2004), the model assumes that the Q cycle, either obligatorily or partially operated, is impartial to cyclic and noncyclic electrons (Allen 2003).

Quantum efficiency of electron transport when cyclic and noncyclic pathways co-occur

When CET and noncyclic (including linear and pseudocyclic) electron transport run simultaneously, a higher electron flux is expected in PSI than in PSII. This means that the fraction of light energy partitioned to PSI and PSII may not be 0.5 each as set by eqn 4 in the canonical FvCB model, but higher than 0.5 for PSI. On the other hand, the partitioning factor must also depend on the photochemical efficiency of the two photosystems, with partitioning in favour of the less efficient PSII in the absence of CET, given that the photochemical efficiency of PSII (Φ_2) is lower than that of PSI (Φ_1) (e.g. Hogewoning et al. 2012). Yin et al. (2004) developed an analytical equation for describing the parameter $\alpha_{2(\mathrm{LL})}$, the quantum efficiency of PSII electron transport (under limiting light, LL) on the basis of absorbed photons by both photosystems:

$$\alpha_{2(\mathrm{LL})} = \frac{\Phi_{2(\mathrm{LL})}(1-f_{\mathrm{cyc}})}{\Phi_{2(\mathrm{LL})}/\Phi_{1(\mathrm{LL})} + (1-f_{\mathrm{cyc}})} \tag{10a}$$

The fraction of absorbed light partitioned to PSII, ρ_2, can be formulated as:

$$\rho_2 = \frac{\alpha_{2(\mathrm{LL})}}{\Phi_{2(\mathrm{LL})}} = \frac{1-f_{\mathrm{cyc}}}{\Phi_{2(\mathrm{LL})}/\Phi_{1(\mathrm{LL})} + (1-f_{\mathrm{cyc}})} \tag{10b}$$

Eqn 10a and eqn 10b both suit for limiting light conditions, as well as for nonlimiting light conditions (if the subscript $_{(\mathrm{LL})}$ is removed) as long as A is limited by electron transport. The model for describing J_2 as a function of the full range of absorbed irradiance (I_{abs}) can be formulated in analogy to eqn 4 as:

$$J_2 = \frac{\alpha_{2\mathrm{LL}} I_{\mathrm{abs}} + J_{2\max} - \sqrt{(\alpha_{2\mathrm{LL}} I_{\mathrm{abs}} + J_{2\max})^2 - 4\theta\alpha_{2\mathrm{LL}} I_{\mathrm{abs}} J_{2\max}}}{2\theta} \tag{11}$$

where J_{2max} is the maximum value of the potential J_2 under saturating irradiance, to differentiate it from J_{max} in eqn 4 that stands for the maximum rate of the potential LET.

Quantum yield of CO_2 uptake and of O_2 evolution

It is convenient to derive the expression for quantum yield of CO_2 uptake ($\Phi_{CO2(LL)}$), from eqn 5, eqn 9a, eqn 10a and eqn 11 in terms of NADPH supply:

$$\Phi_{CO2(LL)} = \frac{\rho_2 \Phi_{2(LL)}\left(1-\frac{f_{pseudo}}{1-f_{cyc}}\right)(C_c-\Gamma_*)}{(4C_c+8\Gamma_*)} = \frac{\Phi_{2(LL)}(1-f_{cyc}-f_{pseudo})(C_c-\Gamma_*)}{[\Phi_{2(LL)}/\Phi_{1(LL)}+(1-f_{cyc})](4C_c+8\Gamma_*)} \quad (12a)$$

Likewise, $\Phi_{CO2(LL)}$ can also be expressed in terms of ATP supply:

$$\Phi_{CO2(LL)} = \frac{\rho_2 \Phi_{2(LL)}(2+f_Q-f_{cyc})(C_c-\Gamma_*)}{h(1-f_{cyc})(3C_c+7\Gamma_*)} = \frac{\Phi_{2(LL)}(2+f_Q-f_{cyc})(C_c-\Gamma_*)}{[\Phi_{2(LL)}/\Phi_{1(LL)}+(1-f_{cyc})]h(3C_c+7\Gamma_*)} \quad (12b)$$

Equivalent equations based on the canonical FvCB model are:

$$\Phi_{CO2(LL)} = \frac{0.5(1-f)(C_c-\Gamma_*)}{4C+8\Gamma_*} \quad (12c)$$

$$\Phi_{CO2(LL)} = \frac{0.5(1-f)(C_c-\Gamma_*)}{4.5C_c+10.5\Gamma_*} \quad (12d)$$

The FvCB model assumes that $\rho_2 = 0.5$. Comparison of eqn 12a and eqn 12c immediately identifies that the f factor in the FvCB model, representing the fraction of I_{abs} unavailable for Calvin-Benson and photorespiratory cycles, can be expressed as: $f = 1 - \Phi_{2LL}[1 - f_{pseudo}/(1 - f_{cyc})]$. In other words, the factor f actually lumps multiple components, including the non-photochemical loss of PSII (Φ_{2LL} known not to be higher than 0.85, Björkman & Demmig 1987), cyclic electron transport (f_{cyc}), and pseudocyclic electron components (f_{pseudo}) that support alternative metabolic processes. Much literature after Farquhar et al. (1980) often only refers to f to correct for spectral quality of the light (e.g. von Caemmerer 2000). While this definition of f reflects the often-reported wavelength dependent photosystems' photochemical efficiencies and absorption by carotenoids and nonphotosynthetic pigments

(e.g. Evans 1987; Hogewoning et al. 2012), it is more difficult to reconcile well with the insights from the extended model.

Photosynthetic quantum yield can also be expressed in terms of O_2 evolution ($\Phi_{O2(LL)}$). The electron requirement in support of both Calvin-Benson and photorespiratory cycles leads to O_2 evolution at PSII from the splitting of H_2O; so, the total O_2 evolved can be expressed as $(1+2\Gamma*/C_c)V_c$. The O_2 uptake by photorespiration consists of (i) one mol O_2 consumed per mol RuBP oxygenation, and (ii) a further one mol O_2 consumed in the conversion of one mol glycolate to one mol glyoxylate by glycolate oxidase in the peroxisome, producing one mol hydrogen peroxide (H_2O_2) which is immediately destroyed by the action of catalase into one mol H_2O and 0.5 mol O_2 (Fig. 1b). So the total O_2 uptake associated with the photorespiratory pathway is 1.5 mol O_2 per mol RuBP oxygenated, which can be expressed as $1.5V_o = (3\Gamma*/C_c)V_c$. Taking these together, the Rubisco-linked net O_2 evolution is $(1-\Gamma*/C_c)V_c$, which is the same as for CO_2 uptake (von Caemmerer 2000).

The Mehler ascorbate peroxidase reaction consumes noncyclic electrons, but its stoichiometry is that for every mol O_2 directly reduced in this reaction, 0.5 mol O_2 is released by superoxide dismutase and 0.5 mol O_2 is evolved through the splitting of H_2O at PSII such that the reaction results in no net O_2 exchange (Asada 1999). In contrast, processes like nitrate reduction, also consuming noncyclic electrons, do result in O_2 evolution. Thus, if photosynthetic quantum yield is expressed in terms of O_2 evolution ($\Phi_{O2(LL)}$), we can break down f_{pseudo} in eqn 12a into two components: one for the Mehler ascorbate peroxidase reaction and one for other basal components, and the latter is no longer needed in the equation for $\Phi_{O2(LL)}$. As the Mehler ascorbate peroxidase reaction acts as a photoprotection mechanism when absorbed light energy exceeds the enzymatic capacity of downstream metabolism (Ort & Baker 2002), this reaction may be negligible under strictly limiting light conditions. Thus, quantum yield of O_2 evolution for the limiting light conditions becomes:

$$\Phi_{\mathrm{O2LL}} = \frac{\Phi_{\mathrm{2LL}}(1-f_{\mathrm{cyc}})(C_{\mathrm{c}}-\Gamma_*)}{[\Phi_{\mathrm{2LL}}/\Phi_{\mathrm{1LL}}+(1-f_{\mathrm{cyc}})](4C_{\mathrm{c}}+8\Gamma_*)} \quad (12e)$$

Using the quantum yield model to infer hard-to-measure parameters

The unique feature of eqn 12e based on the extended model for W_j is that f_{cyc} is in the model for describing NADPH-dependent quantum yield, in contrast to the conventional belief that CET can generate additional ATP and must appear only in equations for the ATP-dependent quantum yield. Parameter f_{cyc} does appear in eqn 12b for the ATP-dependent quantum yield, but eqn 12b includes uncertain parameters f_Q and h in addition to f_{cyc}. Relying on this unique feature and the generally conserved PSII:PSI efficiency ratio, Yin et al. (2006) showed that a hard-to-measure parameter f_{cyc} can be calculated from eqn 12e, based on measurable parameters Φ_{O2LL} and Φ_{2LL} under nonphotorespiratory conditions:

$$f_{\mathrm{cyc}} = \frac{\Phi_{\mathrm{2LL}}-4\Phi_{\mathrm{O2LL}}(1+\Phi_{\mathrm{2LL}}/\Phi_{\mathrm{1LL}})}{\Phi_{\mathrm{2LL}}-4\Phi_{\mathrm{O2LL}}} \quad (13a)$$

A typical Φ_{2LL} based on chlorophyll fluorescence measurements is 0.8 and a typical Φ_{1LL} based on P700 absorption measurements is close to 1.0 or slightly lower (Genty & Harbinson 1996); so, the Φ_{2LL}:Φ_{1LL} ratio is *ca* 0.85. Φ_{O2LL} of C_3 photosynthesis in the absence of photorespiration is *ca* 0.105 (Björkman & Demmig 1987). The solved f_{cyc} from eqn 13a is then *ca* 0.06. This cannot be considered as an absolute estimate, but suggests that very little CET is needed for C_3 photosynthesis, in line with previous reports (e.g. Avenson et al. 2005).

Once f_{cyc} is known, one can calculate another hard-to-measure light-partitioning parameter ρ_2 from eqn 10b. The obtained ρ_2 is *ca* 0.53, close to the assumed value 0.5 in the canonical FvCB model. This indicates that the requirement for a higher partitioning to the less efficient PSII is to some extent balanced by the requirement for a higher partitioning to PSI to run CET. Eqn 10b suggests that ρ_2 equals exactly 0.5 only if the fraction for the noncyclic electron flow, $1-f_{cyc}$, is equal to the Φ_{2LL}:Φ_{1LL} ratio.

By dividing eqn 12a by eqn 12e that assumes no Mehler ascorbate peroxidase reaction for the limiting light condition, one can solve for basal f_{pseudo} from the Φ_{CO2LL}:Φ_{O2LL} ratio:

$$f_{\mathrm{pseudo}} = \left(1 - \frac{\Phi_{\mathrm{CO2LL}}}{\Phi_{\mathrm{O2LL}}}\right)\left(1 - f_{\mathrm{cyc}}\right) \quad (13b)$$

Unlike eqn 13a, eqn 13b applies to both nonphotorespiratory and photorespiratory conditions. A typical value of Φ_{CO2LL} of C_3 photosynthesis under limiting light in the absence of photorespiration is *ca* 0.093 (Long et al. 1993). This gives an estimate of f_{pseudo} being *ca* 0.10. The Φ_{CO2LL}:Φ_{O2LL} ratio is also known as the assimilatory quotient, and the value of its complement, (1 – the ratio), indicates the extent to which electrons are used in support of the processes like nitrogen assimilation (Bloom et al. 1989; Skillman 2008).

Once f_{cyc} and f_{pseudo} are known, likely combinations of f_Q and h can be solved from eqn (8) for C_3 photosynthesis. Using the above estimates of f_{cyc} and f_{pseudo} for the nonphotorespiratory conditions, the solved h is *ca* 3.1 if $f_Q = 0$ and is *ca* 4.67 if $f_Q = 1$. The latter combination is very close to the contemporary belief that the operation of the Q cycle is obligatory (Sacksteder et al. 2000) and the structural data that chloroplast ATP synthase requires 4.67 c subunits or protons to produce one ATP (Seelert et al. 2000; Hahn et al. 2018). However, like the canonical FvCB model, eqn 8 does not account for small amounts of ATP required for starch synthesis and nitrogen assimilation. As ATP for these processes most likely come from chloroplasts (Noctor & Foyer 1998), then the calculated h would approach 4. Energy requirements for nitrogen assimilation will further be discussed next.

Extension 3: Introducing photorespiration-associated nitrogen and C_1 metabolisms

Nitrogen (N) assimilation can be intrinsically linked to the photorespiratory pathway (Bloom 2015). While the electron and ATP requirement associated with re-cycling of the ammonia released by photorespiration is already accounted for (see Introduction), the energy requirement for reduction and assimilation of new nitrogen that enters the leaf is not

accounted for in the canonical FvCB model. *De novo* assimilation of nitrogen in leaves of C_3 plants can arise via the photorespiratory pathway because, as discussed earlier, the photorespiratory intermediate glycine can be diverted from the photorespiratory pathway and used elsewhere for amino acid synthesis, which explains the reversed photosynthetic sensitivity to CO_2 and O_2 (Harley & Sharkey 1991). In addition, serine, a product of glycine decarboxylation in the photorespiratory pathway, can act as a precursor of several other amino acids (Ros et al. 2014). The nitrogen molecules of both glycine and serine, if exported from the photorespiratory pathway for other uses or accumulated temporarily, have to be replenished by *de novo* assimilation of nitrogen; otherwise the pathway cannot be continued. Busch et al. (2018) extended both W_p- and W_j-limited rates of the FvCB model, by following the stoichiometry of energy requirement by both carbon and nitrogen assimilation as well as the stoichiometry for the amino-group balance. More recently, Busch (2020) further extended the model to account for the additional export of glycolate carbon as the photorespiratory pathway is also the main supply of the activated one-carbon units to the so-called C_1 metabolism. This is because, as stated in Introduction, the glycine decarboxylation step can catalyse the conversion of the cofactor tetrahydrofolate (THF) to CH_2-THF that acts as the leaf's currency for activated C_1 units. Here, we collectively describe the extension involving both *de novo* nitrogen assimilation and C_1 metabolisms (Fig. 3).

The general model of Extension 3 integrating nitrogen and C_1 metabolisms

Busch et al. (2018) used α_G and α_S to denote the fractions of glycolate carbon taken out from the photorespiratory pathway as glycine and serine, respectively. Likewise, Busch (2020) used α_T to denote the fraction of glycolate carbon taken out from the photorespiratory pathway as CH_2-THF. As shown in Fig. 3, the glycolate carbon exported in the form of the three-carbon molecule serine has to be $\leq$ the remaining carbon after the glycine export,

glycine decarboxylation, and CH_2-THF export: $\frac{2}{3}\alpha_S \leq \frac{1}{2}(1-\alpha_G)-\alpha_T$, where $\frac{2}{3}$ refers to the glycolate : serine carbon ratio (Fig. 1b), and $\frac{1}{2}$ refers to half of glycine carbon lost during its decarboxylation. This relation can be converted into $\alpha_G + 2\alpha_T + \frac{4}{3}\alpha_S \leq 1$, thereby reflecting that the total proportion of glycolate carbon exports cannot exceed 1. Of course, none of α_G, α_T and α_S can be lower than 0. In analogy to the derivation of eqn 7a by Harley and Sharkey (1991), the rate of P_i consumption, which usually is $(1-0.5\phi)V_c/3$, should be decreased by $(\alpha_G+2\alpha_T+\frac{4}{3}\alpha_S)\phi V_c/2$, and the net P_i consumption would be $[(1-0.5\phi)/3-(\alpha_G+2\alpha_T+\frac{4}{3}\alpha_S)\phi/2]V_c$. Thus, W_p as the rate of carboxylation set by TPU limitation in this case becomes:

$$W_p = \frac{T_p}{(1-0.5\phi)/3-(\alpha_G+2\alpha_T+\frac{4}{3}\alpha_S)\phi/2} = \frac{3T_p}{1-0.5\phi(1+3\alpha_G+6\alpha_T+4\alpha_S)} \quad (14)$$

Eqn 14 becomes eqn 7a if $\alpha_S = 0$ and $\alpha_T = 0$.

While W_c remains unchanged as eqn 2a, the rate of carboxylation as determined by electron transport, W_j, will be affected as the potential electron transport rate J now has to support both carbon and nitrogen assimilation. Photorespiratory carbon entering the C_1 metabolism, in contrast, causes a net release of electrons, as the reaction catalysed by GDC releases electrons and the exit of carbon from the photorespiratory pathway saves electrons downstream that would otherwise be consumed for converting serine to glycerate in the peroxisome and for reducing this glycerate-derived 3-PGA in the chloroplast (Fig. 1b; Fig. 3). These together bring the equation for electron transport-determined carboxylation rate in terms of NADPH supply to:

$$W_j = \frac{J}{4+(4+8\alpha_G-4\alpha_T+4\alpha_S)\phi} \quad (15a)$$

The denominator can be obtained by summing up all the electron requirements for individual steps, deducted by electron equivalents of the NADH release as a result of glycine decarboxylation, indicated in Fig. 3. Likewise, photorespiratory carbon export via the C_1

metabolism saves ATP that would otherwsie be used for the phosphorylation of glycerate to 3-PGA and for the subsequent phosphorylation of this 3-PGA (Fig. 1b; Fig. 3); thus, one can formulate the equation for W_j in terms of ATP supply:

$$W_j = \frac{J_{atp}}{3+(3.5-0.5\alpha_G-\alpha_T-\frac{2}{3}\alpha_S)\phi} \quad (15b)$$

where J_{atp} in the numerator is the total ATP production rate from chloroplastic electron transport (which is not expressed in J like eqn 15a, given the uncertainties discussed earlier in Extension 2). The denominator in eqn 15b can also be obtained by summing up all the ATP requirements indicated in Fig. 3.

Traditionally, the proportion of glycolate carbon that does not return to chloroplasts (α) is relevant only for the TPU-limited carboxylation rate W_p (see eqns 7a,b). Eqns 15a,b suggest that the proportion parameters (α_G, α_T and α_S) affect not only W_p but also W_j. The export of carbon as CH_2-THF always increases W_j. Glycine and serine export associated with *de novo* N assimilation decreases W_j in terms of NADPH requirement whereas it increases W_j in terms of ATP requirement. This suggests that photorespiration-associated N assimilation can help alleviate the deficit of ATP relative to NADPH (see earlier discussions).

In the case of glycine being diverted from the photorespiratory pathway, the amount of CO_2 released per oxygenation should be decreased by α_G (Busch et al. 2018). In contrast, as shown in Fig. 3, every carbon exported as CH_2-THF from the pathway results in one carbon lost from glycine decarboxylation (Busch 2020). Therefore, it is necessary to revise eqn 1 to:

$$A = V_c - [0.5(1-\alpha_G)+\alpha_T]V_o - R_d \quad (16a)$$

And eqn 6a becomes:

$$A = \left(1-\frac{\Gamma_{*GT}}{C_c}\right)\min(W_c, W_j, W_p) - R_d \quad (16b)$$

where $\Gamma_{*GT} = [0.5(1-\alpha_G)+\alpha_T]O/S_{c/o}$, or $\Gamma_{*GT} = (1-\alpha_G+2\alpha_T)\Gamma_*$. It follows that the CO_2 compensation point in the absence of day respiration is no longer constant at given

temperature and O_2 partial pressure, but decreases with increasing the fraction of glycine and increases with increasing the fraction of CH_2-THF diverted from the photorespiratory pathway. Therefore, equations for the net CO_2-assimilation rate corresponding to the three limitations become:

$$A_{\mathrm{c}} = \frac{\{1-[0.5(1-\alpha_{\mathrm{G}})+\alpha_{\mathrm{T}}]\phi\}(C_{\mathrm{c}}V_{\mathrm{cmax}})}{C_{\mathrm{c}}+K_{\mathrm{mC}}(1+O/K_{\mathrm{mO}})} - R_{\mathrm{d}} = \frac{[C_{\mathrm{c}}-\Gamma_*(1-\alpha_{\mathrm{G}}+2\alpha_{\mathrm{T}})]V_{\mathrm{cmax}}}{C_{\mathrm{c}}+K_{\mathrm{mC}}(1+O/K_{\mathrm{mO}})} - R_{\mathrm{d}} \quad (16c)$$

$$A_{\mathrm{j}} = \frac{\{1-[0.5(1-\alpha_{\mathrm{G}})+\alpha_{\mathrm{T}}]\phi\}J}{4+(4+8\alpha_{\mathrm{G}}-4\alpha_{\mathrm{T}}+4\alpha_{\mathrm{S}})\phi} - R_{\mathrm{d}} = \frac{[C_{\mathrm{c}}-\Gamma_*(1-\alpha_{\mathrm{G}}+2\alpha_{\mathrm{T}})](J/4)}{C_{\mathrm{c}}+(1+2\alpha_{\mathrm{G}}-\alpha_{\mathrm{T}}+\alpha_{\mathrm{S}})(2\Gamma_*)} - R_{\mathrm{d}} \quad (16d)$$

$$A_{\mathrm{p}} = \frac{\{1-[0.5(1-\alpha_{\mathrm{G}})+\alpha_{\mathrm{T}}]\phi\}(3T_{\mathrm{p}})}{1-0.5\phi(1+3\alpha_{\mathrm{G}}+6\alpha_{\mathrm{T}}+4\alpha_{\mathrm{S}})} - R_{\mathrm{d}} = \frac{[C_{\mathrm{c}}-\Gamma_*(1-\alpha_{\mathrm{G}}+2\alpha_{\mathrm{T}})](3T_{\mathrm{p}})}{C_{\mathrm{c}}-(1+3\alpha_{\mathrm{G}}+6\alpha_{\mathrm{T}}+4\alpha_{\mathrm{S}})\Gamma_*} - R_{\mathrm{d}} \quad (16e)$$

Applying quantitative isotopic techniques to sunflower leaves, Abadie et al. (2016) showed that the stoichiometric ratio of O_2 fixation by Rubisco to CO_2 production by GDC increased from 2.0 (the theoretical value used in the canonical FvCB model) at very low-photorespiration gas mixtures, to 2.05 for the normal ambient condition, and to 2.09 to high-photorespiration gas mixtures. As the export of carbon in the form of CH_2-THF would make this ratio lower than 2.0, the observed ratio being ≥2.0 suggests that the export of carbon from the photorespiratory pathway via this form may be less important than the export via glycine. If the value of > 2.0 is due to glycine export alone, then α_{G} can be estimated to be 0.0 for the conditions with little photorespiration, 0.024 for the ambient condition, and a maximum value of 0.043 for the conditions of high-photorespiration gas mixture. Using modelling to fit eqns 16c-e to A-C_{i} curves, Busch et al. (2018) estimated α_{G} of the ambient condition to be 0.026 for plants fed with NH_4^+-N, 0.103 for plants fed with NO_3^--N, and 0.077 for control plants. These all indicate that α_{G} is not zero as implicitly assumed in the canonical FvCB model. This means that even under Rubisco limitation where W_{c} is not changed by any amino acid export, A could still be increased due to a slight decrease in the CO_2-compensation point if glycine is removed from the photorespiratory pathway (see eqn 16c). Under the TPU limitation where carbon uptake is limited by the rate at which carbohydrates can be metabolised, A could be

further increased by short-circuiting carbon flux to glycine, serine, and CH_2-THF via the photorespiratory pathway. Only the NADPH-dependent electron transport-limited rate is decreased due to the electron consumption by the *de novo* nitrogen assimilation (if the potential electron transport rate J remains the same; but see later discussion).

In addition to exploring the ratio of O_2 fixation by Rubisco to CO_2 production by GDC to estimate α_G, Busch et al. (2018) showed that α_G and α_S could be roughly estimated from model fitting to A-C_i curves. There is currently no information available about the possible value for the fraction of glycolate carbon diverted via the C_1 metabolism (Busch 2020). Therefore, hereafter we mainly discuss the relations with regard to the amino-acid exports.

Relationships with the previous two extensions

It is clear, based on the model of Busch et al. (2018), that the parameter α in the model of Harley & Sharkey (1991) deals with the carbon side of the amino acid export but not the electron requirement for NO_3^- assimilation. In addition, the energy associated with the changed RuBP regeneration and NH_4^+-recycling as a result of amino acid export was not considered in Harley & Sharkey's model. Also, the decrease of CO_2-compensation point in the absence of R_d as a result of the glycine exit is not explicitly included in the model although this was discussed by Harley & Sharkey (1991). Busch et al. (2018) treated amino acid exit from the photorespiratory pathway differently, depending on whether it is glycine or serine that is exited, whereas Harley & Sharkey (1991) only assumed the glycine exit. It is clear from eqn 16e that if it is only glycine that exits, the model under a TPU-limitation is:

$$A_p = \frac{[C_c - \Gamma_*(1-\alpha_G)](3T_p)}{C_c - (1+3\alpha_G)\Gamma_*} - R_d \quad (17a)$$

If the CO_2-compensation point is to be maintained as in the canonical FvCB model, it would be internally consistent to assume that it is only serine, instead of glycine, being exported. Then, based on eqn 16e, the model for A under a TPU-limitation should become:

$$A_{\mathrm{p}} = \frac{(C_{\mathrm{c}} - \Gamma_*)(3T_{\mathrm{p}})}{C_{\mathrm{c}} - (1+4\alpha_{\mathrm{S}})\Gamma_*} - R_{\mathrm{d}} \quad (17b)$$

with the bound that $0 \leq \alpha_S \leq 0.75$. This model is supported by the above calculation that α_G was maximally only 0.043 based on isotopic measurements of Abadie et al. (2016) as well as by the modelling result of Busch et al. (2018) and measurements of Abadie et al. (2018) that α_S was often much higher than α_G, reflecting high demands for serine due to its important role in the one-carbon metabolism and as precursor for several other amino acids and phospholipids (Ros et al. 2014). Previous parameterisation of eqn 7b from fitting to A-C_i curves with a moderate reverse sensitivity to C_i increases showed that the estimated α was as high as 0.77 (Busch et al. 2018), partly being the artefact of ignoring the decrease of CO_2-compensation point by eqn 7b, thereby exaggerating the actual fraction of glycolate carbon not returned to the chloroplast. This fraction would decrease by 25% if eqn 17b is used. In fact, using the same total fraction of glycolate carbon not returned to the chloroplast, eqn 17a and 17b generates nearly identical curves as the full TPU-limitation model eqn 16e without the α_T terms (Fig. 4), whereas eqn 7b generates much lower values. As Fig. 4 demonstrates, there is little signal to differentiate α_G and α_S by conventional gas exchange (McClain & Sharkey 2019), but only the sum of the two can be reliably estimated. Therefore, if α_G and α_S are to be estimated one cannot rely on eqn 16e alone, but needs to consider at the very minimum the full range of A-C_i response fitted with eqn 16b and include measurements of the compensation point, which is affected by α_G but not by α_S.

It is also possible to connect the model of Busch et al. (2018) with the model of Yin et al. (2004). As stated earlier, parameter f_{pseudo} in the model of Yin et al. (2004) can largely reflect the proportion of electrons for supporting nitrogen assimilation, especially under electron transport-limited conditions. Thus, one can equate eqn 16d without the α_T terms to A_j formulated from eqn 9a:

$$\frac{[1-0.5\phi(1-\alpha_G)]J}{4+(4+8\alpha_G+4\alpha_S)\phi} = \left(1-\frac{f_{pseudo}}{1-f_{cyc}}\right)\frac{(1-0.5\phi)J_2}{4+4\phi} \quad (18a)$$

Note that J on the left side of the equation must be equal to J_2 on the right side, as they both represent the rate of whole-chain electron transport in support of the Calvin-Benson cycle, the photorespiratory pathway and nitrogen assimilation (in this context, J in the model of Busch et al. 2018 actually differs from J in the canonical FvCB model). Solving for f_{pseudo} gives:

$$f_{pseudo} = \left\{\frac{(8\alpha_G+4\alpha_S)\phi(1-0.5\phi)-0.5\phi\alpha_G(4+4\phi)}{[4+(4+8\alpha_G+4\alpha_S)\phi](1-0.5\phi)}\right\}(1-f_{cyc}) \quad (18b)$$

As stated earlier, f_{cyc} for C_3 photosynthesis is negligible (set to nil here). The modelling by Busch et al. (2018) showed that for the ambient-air condition, α_G was *ca* 0.10 and α_S was *ca* 0.15 for plants fed with NO_3^--N. Assuming $\phi = 0.3$ for the ambient condition, then 0.058 for f_{pseudo} can be calculated from eqn 18b. This value would become even lower if there are small amounts of CET. For nonphotorespiratory conditions ($\phi = 0$), eqn 18b gives that $f_{pseudo} = 0$.

Eqn 18b also reveals that surprisingly f_{pseudo} does not increase monotonically with increasing ϕ if ϕ goes to a very high value (Fig. 5a). The decline of f_{pseudo} beyond a threshold ϕ occurs only in the presence of α_G; and the higher is α_G, the lower is the threshold ϕ. However, f_{pseudo} always increases monotonically with increasing ϕ in the absence of α_G, regardless of values of α_S. All these responses are because α_G, not α_S, causes a decrease in CO_2-compensation point, and this positive impact on A becomes increasingly important under high photorespiratory states (high ϕ values) that mathematically requires a low f_{pseudo} to enable the left and right sides of eqn 18a in balance. For the same reason, although f_{pseudo} generally increases with increasing α_G or α_S, its response to α_G is stronger than to α_S at a low ϕ (Fig. 5b), is comparable at an intermediate ϕ corresponding to ambient-air conditions (Fig. 5c), and is weaker than to α_S at a high ϕ (Fig. 5d).

It is noteworthy that f_{pseudo} calculated from eqn 18b refers to the electron fraction responsible for supporting N assimilation only as result of amino acid export from the

photorespiratory pathway. Therefore, the calculated f_{pseudo} depends on the amount of photorespiration as shown in Fig. 5. In contrast, f_{pseudo} as one parameter in the model of Yin et al (2004) for electron-transport-limited conditions lumps electron requirements for: (i) N assimilation of both via the photorespiratory pathway and not via this pathway and (ii) metabolic processes other than N assimilation that utilise chloroplastic electrons. As stated earlier, f_{pseudo} of *ca* 0.10 was estimated from the assimilatory quotient for nonphotorespiratory conditions. The higher f_{pseudo} estimated from the assimilatory quotient suggests that either not all nitrogen is assimilated via the photorespiratory pathway or/and processes other than N assimilation consumes chloroplastic electrons. Furthermore, the model of Busch et al. (2018) only applies to the case where it is NO_3^--N that enters the leaf. However, it cannot be ruled out that nitrogen enters the leaf in the form of NH_4^+-N (Eichelmann et al. 2011), and for such a case the stoichiometric coefficients of eqn 15a has to be re-formulated whereas the model of Yin et al. (2004) remains the same but with a lower value of f_{pseudo}.

The FvCB model coupled with the mesophyll CO_2-diffusion model

While C_i (intercellular CO_2 partial pressure) was used in the FvCB model at the time when this model was initially published, it is increasingly recognised that C_c should be used because the resistance of CO_2 diffusion from intercellular-air spaces (IAS) to the chloroplast stroma of mesophyll cells cannot be ignored. This resistance is called mesophyll resistance (r_m), while its inverse is called mesophyll conductance (g_m), and has long been defined as such that the C_i-to-C_c gradient can be expressed (von Caemmerer & Evans 1991):

$$C_c = C_i - Ar_m = C_i - A/g_m \quad (19a)$$

Because A is the difference between carboxylation rate (V_c) and the rate of CO_2 release from photorespiration ($F = 0.5V_o$ or $[0.5(1-\alpha_G) + \alpha_T]V_o$) and respiration ($R_d$), eqn 19a implicitly assumes that the CO_2 coming from IAS and the CO_2 released from

(photo)respiration experience the same resistance r_m. To diffuse to Rubisco, the CO_2 coming from IAS has to experience the resistance across mesophyll cell wall and plasma membrane (r_{wp}) as well as the resistance across the chloroplast envelope and inside the chloroplast stroma (r_{ch}). In contrast, the (photo)respiratory CO_2 first enters the cytosol after being released by the mitochondria and therefore, if to be re-fixed by Rubisco, may experience r_{ch} only. For this reason, Tholen et al. (2012) presented a resistance model that explicitly differentiates the resistances faced by the two different sources of CO_2:

$$C_c = C_i - Ar_m - (F + R_d)r_{ch} \quad (19b)$$

where $r_m = r_{wp}+r_{ch}$. If the chloroplast resistance is negligible ($r_{ch} \to 0$), then eqn 19b becomes eqn 19a. Clearly, the earlier model, eqn 19a, also assumes that the chloroplast resistance is negligible so that only r_{wp} forms the mesophyll resistance as if RuBP carboxylation and (photo)respiratory CO_2 production occur in the same compartment.

Equations (19a) and (19b) have been considered as two basic scenarios for CO_2 diffusion path in C_3 leaves (von Caemmerer 2013). However, the delivery of CO_2 to Rubisco depends not only on simple physical resistance components but also on the intracellular arrangement of organelles that consume and produce CO_2. Yin & Struik (2017b) considered six scenarios of the arrangement of mitochondria and chloroplasts, and came up with a generic model:

$$C_c = C_i - Ar_m - (1 - k\lambda)(F + R_d)r_{ch} \quad (19c)$$

where λ is the fraction of mitochondria that locate closely behind chloroplasts in the inner cytosol (i.e. the area between chloroplasts and vacuole; then $1-\lambda$ is the fraction of mitochondria that locate in the outer cytosol, the area between the plasma membrane and chloroplasts), and k is a factor allowing the fraction of (photo)respiratory CO_2 in the inner cytosol dependent not only on λ but also on chloroplast gaps and the cytosol resistance. So, the term $k\lambda$ can be regarded as the fraction of (photo)respiratory CO_2 in the inner cytosol. If

$k\lambda = 1$, eqn 19c becomes eqn 19a, meaning that eqn 19a also implicitly assumes that mitochondria exclusively lie behind chloroplasts that form a continuum without a gap as observed for rice (Sage & Sage 2009). If $k\lambda = 0$, eqn 19c becomes eqn 19b, meaning that eqn 19b applies to the case where mitochondria exclusively lie in the outer cytosol ($\lambda = 0$) with chloroplasts that form a continuum without a gap ($k = 1$) or to the case where there are chloroplast gaps but little cytosol resistance ($k = 0$), and thus photorespiratory CO_2 anywhere in the cytosol is completely mixed, independent of where the mitochondria are located. Eqn 19a and eqn 19b represent two extremes, and the reality should be somewhere in-between ($0 < k\lambda < 1$). Eqn 19c can be further simplified to:

$$C_c = C_i - [A + m(F + R_d)]r_m \tag{19d}$$

where parameter m lumps several parameters: $m = (1-\lambda k)r_{ch}/r_m$ and $0 \le m \le 1$ (also see Ubierna et al. 2019).

Combining the above forms of equations for r_m or g_m with the (extended) FvCB model and solving for A can lead to an expression that models A as a function of C_i (von Caemmerer et al. 1994; Ethier & Livingston 2004; von Caemmerer 2013; Yin & Struik 2017b). Here, based on the model of Yin et al. (2020), we present a form that covers all possibilities:

$$A = \frac{-b' \pm \sqrt{b'^2 - 4a'c'}}{2a'} \tag{20}$$

where $a' = x_2 + \Gamma_{*GT}(1-m) + \delta(C_i + x_2)$

$$b' = m(R_d x_2 + \Gamma_{*GT} x_1) - [x_2 + \Gamma_{*GT}(1-m)](x_1 - R_d) - (C_i + x_2)[g_{mo}(x_2 + \Gamma_{*GT}) + \delta(x_1 - R_d)] - \delta[x_1(C_i - \Gamma_{*GT}) - R_d(C_i + x_2)]$$

$$c' = -m(R_d x_2 + \Gamma_{*GT} x_1)(x_1 - R_d) + [g_{mo}(x_2 + \Gamma_{*GT}) + \delta(x_1 - R_d)][x_1(C_i - \Gamma_{*GT}) - R_d(C_i + x_2)]$$

and $$x_1 = \begin{cases} V_{cmax} & \text{for } W_c\text{-limited} \\ J/4 & \text{for } W_j\text{-limited} \\ 3T_p & \text{for } W_p\text{-limited} \end{cases},$$

$$x_2 = \begin{cases} K_{\mathrm{mC}}(1 + O/K_{\mathrm{mO}}) & \text{for } W_{\mathrm{c}}\text{-limited} \\ (1 + 2\alpha_{\mathrm{G}} - \alpha_{\mathrm{T}} + \alpha_{\mathrm{S}})(2\Gamma_*) & \text{for } W_{\mathrm{j}}\text{-limited} \\ -(1 + 3\alpha_{\mathrm{G}} + 6\alpha_{\mathrm{T}} + 4\alpha_{\mathrm{S}})\Gamma_* & \text{for } W_{\mathrm{p}}\text{-limited} \end{cases}$$

Whether or not g_m is variable is still under debate (Evans 2021); in particular, Gu & Sun (2014) showed that the variable g_m pattern could be an artefactual response to uncertainties in measurements or in estimating parameters of the FvCB model. But eqn 20 suits for either a constant or a variable g_m mode. Setting $\delta = 0$ would make eqn 20 appropriate the constant g_m mode (= g_{mo} of eqn 20). Setting $g_{mo} = 0$, then a positive value of δ, which defines the carboxylation resistance : mesophyll resistance ratio (Yin et al. 2020), allows the possibility that g_m is variable, responding to C_i, irradiance, temperature, and O_2 as reported by, e.g. Bernacchi et al. (2002), Flexas et al. (2007) and Yin et al. (2020). In eqn 20, Γ_{*GT} is used in several places, instead of the usual Γ_*, to account for the earlier discussed possible change in CO_2 compensation point due to the carbon exit via glycine and CH_2-THF from the photorespiratory pathway. It is worthy to note that while the complete form of the equations for x_2 in case of the W_j-limitation is given, usually only $x_2 = 2\Gamma_*$ is applied, especially if the model is used to estimate g_m.

The solution to eqn 20 in case of W_c or W_j limitations is straightforward (the $\sqrt{b'^2 - 4a'c'}$ term always taking the – sign). Gu et al. (2010) highlighted the mathematical complication arisen from a negative x_2 in the case that W_p limits if the fraction of glycolate carbon not returned to chloroplasts is > 0 and suggested a solution to that.

The coupled g_m-FvCB model offers a method to estimate g_m (and other parameters) by fitting to gas exchange data only from exploring the curvature of A-C_i curves (Ethier & Livingston 2004). When the coupled model is fitted to combined gas exchange and chlorophyll fluorescence data (Yin & Struik 2009), it can improve the reliability of the estimates compared with the value of g_m calculated from the conventional variable J method of Harley et al. (1992). An alternative is using the stable ^{13}C-isotope discrimination method

(Farquhar et al. 1982), which was applied by Evans et al. (1986; 1994) to estimate g_m (see review by Pons et al. 2009, and the most current model by Busch et al. 2020). But the chlorophyll fluorescence-based methods are more widely used because of the wider availability of the required device, despite the limitations (Evans 2021). To minimise the influence of these limitations and of basal alternative transport pathways on estimating g_m, van der Putten et al. (2018) demonstrated the importance of calibration using the measurements under nonphotorespiratory conditions. Any calibration method assumes that the fractions for alternative electron pathways are constant between photorespiratory and nonphotorespiratory conditions. However, recent reports by Abadie et al. (2016, 2018, 2019) and Tcherkez & Limami (2019) suggest that the values of α_G and α_S, as well as the percentage of phospho*enol*pyruvate (PEP) carboxylation and malate production (if any), and N-assimilation relative to CO_2-assimilation may not be constant across various CO_2/O_2 gas mixtures. Chlorophyll-fluorescence-based methods to estimate g_m require data that include the measurements under photorespiratory conditions such as at ambient CO_2/O_2 levels (Yin et al. 2020) whereas the ^{13}C isotopic method has no such a requirement. On the other hand, estimates of g_m by the ^{13}C isotopic method are affected by assumptions made regarding the values of the fractionation factors (Pons et al. 2009; Gu & Sun 2014; Busch et al. 2020). Thus, chlorophyll-fluorescence and ^{13}C isotopic methods should be compared, whenever possible, for estimating g_m.

As the chlorophyll-fluorescence-based method relies on the coupled g_m-FvCB model and the re-assimilation of photorespired CO_2 to estimate g_m, this coupled model should account for the amount of (photo)respired CO_2 that are re-assimilated by Rubisco. For example, let us assume two hypothetical leaves where all parameters are the same except R_d which is nil for one leaf vs 3 μmol m^{-2} s^{-1} for the other. One would expect from the C_c-based model, e.g. eqns 16c,d,e, that A also differs by 3 μmol m^{-2} s^{-1} between the two leaves. However, the calculation

using the coupled model shows that the difference in A was smaller than the difference in R_d of 3 μmol m^{-2} s^{-1} (Fig. 6a) because part of CO_2 released by day respiration in the second leaf is re-assimilated by Rubisco, demonstrating that the refixation is implicitly accounted for by the coupled model. The lower is g_m, the harder it is for the (photo)respired CO_2 to escape, and the higher is the proportion of refixation (Fig. 6a). The calculated refixation proportion varies little with the assumed R_d values of the two leaves. In fact, the fraction of (photo)respired CO_2 being refixed (f_{refix}) can be calculated directly using the resistance components (Tholen et al. 2012). They proposed an equation for the scenario which eqn 19b represents. Yin & Struik (2017b) extended the approach to a general equation:

$$f_{\mathrm{refix}} = \frac{\frac{\lambda k}{r_{\mathrm{cx}}} + \frac{1-\lambda k}{r_{\mathrm{ch}}+r_{\mathrm{cx}}}}{\frac{\lambda k}{r_{\mathrm{cx}}} + \frac{1-\lambda k}{r_{\mathrm{ch}}+r_{\mathrm{cx}}} + \frac{\lambda k}{r_{\mathrm{wp}}+r_{\mathrm{ch}}+r_{\mathrm{sc}}} + \frac{1-\lambda k}{r_{\mathrm{wp}}+r_{\mathrm{sc}}}} \tag{21a}$$

where r_{sc} is the stomatal resistance to CO_2 diffusion, and r_{cx} is the resistance from the carboxylation reaction itself, which can be defined as: $(C_c+x_2)/x_1$ (von Caemmerer 2000; 2013) and was similarly as high as r_m (= $r_{wp}+r_{ch}$) in rice leaves and *ca* 40% higher than r_m in tomato leaves (Yin et al. 2020). If $\lambda k = 1$, eqn 21a is simplified to:

$$f_{\mathrm{refix}} = \frac{r_{\mathrm{sc}}+r_{\mathrm{wp}}+r_{\mathrm{ch}}}{r_{\mathrm{sc}}+r_{\mathrm{wp}}+r_{\mathrm{ch}}+r_{\mathrm{cx}}} \tag{21b}$$

If $\lambda k = 0$, eqn 21a becomes eqn 14 of Tholen et al. (2012):

$$f_{\mathrm{refix}} = \frac{r_{\mathrm{sc}}+r_{\mathrm{wp}}}{r_{\mathrm{sc}}+r_{\mathrm{wp}}+r_{\mathrm{ch}}+r_{\mathrm{cx}}} \tag{21c}$$

It becomes obvious from eqns 21b,c that leaves having the anatomical structure close to what eqn 19a describes have a higher f_{refix} than leaves having the structure that eqn 19b describes, and this difference in f_{refix} leads to different CO_2 compensation points (von Caemmerer 2013; Yin & Struik 2017b). As r_{sc} and r_{cx} vary in response to CO_2, irradiance and other environmental conditions, it follows that the proportion of (photo)respired CO_2 being refixed varies with these variables. For example, with an increase of CO_2, r_{cx} [= $(C_c+x_2)/x_1$)] will increase, and eqns 21b,c will predict a decrease of f_{refix}, in line with the expectation that

refixation contributes decreasingly to total assimilation with increasing CO_2 (Busch et al. 2013). This appears to agree with the result in Fig. 6a that with increasing C_i, calculated differences in A approach to the preset difference in R_d.

Refixation can occur both within the mesophyll cell ($f_{refix,cell}$) and via the IAS ($f_{refix,ias}$), which together constitute the total refixation ($f_{refix} = f_{refix,cell} + f_{refix,ias}$) (Busch et al. 2013). In fact, the refixation of R_d illustrated in the above example using the coupled model with C_i as input (Fig. 6a) actually refers to $f_{refix,cell}$. $f_{refix,cell}$ and $f_{refix,ias}$ can also be directly calculated from resistance components and Yin et al. (2020) showed that if the term r_{sc} is removed, eqns 21a-c become equivalent equations to calculate $f_{refix,cell}$. They showed that $f_{refix,cell}$ generally dominates and leaves having the anatomical structure that eqn 19a describes have a higher $f_{refix,cell}$ and thus a higher f_{refix} than leaves having the structure that eqn 19b describes despite the latter leaves having a higher $f_{refix,ias}$. They quantitatively showed that for rice leaves where $\lambda k = 1$, the estimated f_{refix} was often high (≥ 0.5). These ideas of refixation have been exploited by synthetic biology approaches that engineer photorespiratory bypasses to relocate the photorespiratory CO_2 release from mitochondria to chloroplasts (Kebeish et al. 2007; Shen et al. 2019; South et al. 2019; Fig. 1a). The bypasses may be effective in increasing CO_2 assimilation for leaves described by eqn 19b under low CO_2 conditions. However, values calculated based on resistance components represent the gross refixation of (photo)respired CO_2, which is higher than the refixation reflected by results of the coupled model (Fig. 6b). This suggests (photo)respired CO_2 or bypassed CO_2 decrease the chance of CO_2 coming from IAS being assimilated; so, the net benefit of refixation must be smaller than what eqns 21a-c predict. But the bypass-associated saving of electrons and ATP that otherwise are consumed by the ammonia recycling (Fig. 1a) provides more advantages (von Caemmerer 2013).

The C_4 form of the FvCB model

CO_2 diffusion is also important for C_4 photosynthesis because its CO_2-concentrating mechanism (CCM) relies on the effective coordination of a series of diffusional processes and biochemical reactions. In the vast majority of terrestrial C_4 species, this mechanism is achieved through the coordinated functioning via the Kranz structure involving mesophyll (M) and bundle-sheath (BS) cells (Hatch 1987). CO_2 initially diffuses to the M cytosol and is converted to HCO_3^-, which is fixed by PEP carboxylase (PEPc) into C_4 acids. The C_4 acids travel to the BS cells, where they are decarboxylated and the released CO_2 is re-fixed by Rubisco exclusively localised in BS chloroplasts. The K_m of PEPc is lower, and its maximum carboxylation rate is generally higher, than that of Rubisco. This will elevate the CO_2 partial pressure in the BS compartment, despite some leakage of CO_2 from BS back to M cells, which effectively suppresses photorespiration. Because Rubisco is operated in high-CO_2 compartments, kinetic constants of C_4 Rubisco differ from those of C_3 Rubisco (Cousins et al. 2010; Boyd et al. 2015; Sharwood et al. 2016), which together with the CCM *per se*, underlies the high photosynthetic nitrogen use efficiency of C_4 plants (Ghannoum et al. 2005). C_4 species are traditionally classified into three subtypes according to the decarboxylation enzymes, thus also decarboxylation sites: NADP-malic enzyme (ME) in chloroplasts, NAD-ME in mitochondria, and PEP-carboxykinase (CK) in the cytosol (Hatch 1987). However, more recent opinions (e.g. Furbank 2011; Wang et al. 2014; Yin & Struik 2018) suggest that C_4 species often have a mixed decarboxylation pathway, where one enzyme acts as the main decarboxylating enzyme alongside the others.

The standard model for C_4 photosynthesis

Berry & Farquhar (1978) presented a first model for C_4 photosynthesis, which covered the CCM and the basis of high nitrogen use efficiency. The leakiness (ϕ_L) as the ratio of the CO_2 retro-leakage (L) to the rate of PEP carboxylation (V_p), was introduced in a model that

included carbon isotope discrimination (Farquhar 1983). Based on these earlier models, von Caemmerer & Furbank (1999) described a model, which is now considered as the standard C_4 model that predicts net CO_2-assimilation rate (A) as a function of mesophyll cytosol CO_2 partial pressure (C_m). Several equations relevant to the C_4 photosynthesis are:

- the flux balance in the M cell: $A = V_p - L - R_m$ (22a)

- the rate of CO_2 leakage: $L = g_{bs}(C_c - C_m)$ (22b)

- the level of O_2 in the BS cell: $O_c = \alpha_{bs} A/(u_{oc} g_{bs}) + O_m$ (22c)

- the rate of PEP carboxylation: $V_p = \frac{C_m V_{pmax}}{C_m + K_p}$ or $= \frac{x J_{atp}}{\varphi}$ (22d)

where R_m is the respiration in the M cell (usually assumed to be $0.5R_d$), g_{bs} is bundle-sheath conductance, C_c and O_c are the partial pressure of CO_2 and O_2 at the active sites of Rubisco, respectively, α_{bs} is the fraction of O_2 evolution (or of PSII) in the BS cells, u_{oc} is the coefficient that lumps diffusivities of O_2 and CO_2 in water and their respective Henry constants, O_m is the partial pressure of O_2 at the mesophyll cytosol, K_p and V_{pmax} are the Michaelis-Menten constant and the maximum carboxylation rate of PEPc, respectively, x is the fraction of ATP consumed by the CCM cycle, φ is the mol chloroplastic ATP required for the CCM cycle, and J_{atp} is the rate of ATP production by chloroplastic electron transport. The original model of von Caemmerer & Furbank (1999) did not use J_{atp}, but the rate of electron transport (J). Because it is ATP, not electrons, that are allocated between the CCM cycle and the Calvin-Benson cycle, according to the predefined stoichiometric fraction x, it is more appropriate to use J_{atp} in eqn 22d (Yin et al. 2011) and J_{atp} can be linked with electron transport rate via the ATP production factor z (see eqn 9e). Eqn 22d for V_p contains either the PEPc activity-limited rate or the electron transport-limited rate, in analogy to the equations for V_c. The rate of CO_2-assimilation (A) based on V_c is the same for C_3 photosynthesis and can be collectively expressed as:

$$A = \frac{(C_c - \gamma_* O_c) x_1}{C_c + O_c x_2 + x_3} - R_d \quad (22e)$$

where $\gamma_* = 0.5/S_{c/o}$, and $x_1 = V_{cmax}$, $x_2 = K_{mC}/K_{mO}$, and $x_3 = K_{mC}$ for the Rubisco-limited rate. For the RuBP regeneration-limited rate, $x_1 = (1-x)J_{atp}/3$, $x_2 = 7\gamma_*/3$, and $x_3 = 0$ if ATP supply is limiting. von Caemmerer & Furbank (1999) provided a solution to the combined eqns 22a-e that expresses A as a quadratic function of C_m. As C_m is unknown generally, one may add an equation ($C_m = C_i - A/g_m$) in order to express A as a function of C_i. Yin et al. (2011) provided the analytical solution to these, which became cubic if PEPc activity limits V_p.

Unlike in C_3 leaves, the initial carbon fixation in C_4 leaves is catalysed by PEPc in the cytosol and therefore g_m does not involve CO_2 diffusion from the cytosol to the chloroplast. Accordingly, estimates of g_m in C_4 leaves are somewhat higher than those in C_3 leaves (Barbour et al. 2016), meaning g_m appears to be less limiting to C_4 photosynthesis as it is to C_3 photosynthesis. However, g_{bs}, which determines the amount of CO_2 leakage (see eqn 22b), is fundamentally important for the CCM, and thus, for determining C_4 photosynthesis. So far there is no method that can directly estimate g_{bs}. Its indirect estimate, mostly based on model fitting to gas exchange data (He & Edwards 1996) and sometimes combined with chlorophyll fluorescence or ^{13}C discrimination measurements, suggests a value between 1.0 and 10.0 mmol m^{-2} s^{-1} bar^{-1} (Yin et al. 2011), *ca* two- or three-order of magnitude smaller than g_m. Like g_m, g_{bs} varies with leaf age or N content (Yin et al. 2011), temperature (Kiirats et al. 2002; Yin et al. 2016; Alonso-Cantabrana et al. 2018), and growth light conditions (Kromdijk et al. 2010; Ubierna et al. 2013; Bellasio & Griffins 2014). Danila et al. (2021) showed that suberization of the BS lamellae is required for a low g_{bs} to minimise leakage. As g_{bs} is a lumped model parameter, its value may depend on other anatomical characteristics (like BS cell wall thickness, plasmodesmata density, bundle sheath surface area-to-leaf area ratio, intervein spacing, sheath layers) as well as biochemical characteristics (like the location of decarboxylation). Further research is needed to clarify how these characteristics influence g_{bs}.

Energetic aspects of C_4 photosynthesis

Although energy production or consumption can be cell-type specific (Yin & Struik 2018, 2021), the model of von Caemmerer & Furbank (1999) for C_4 photosynthesis assumed that energy is shared between M and BS cells, and used x to allocate J_{atp} to the CCM cycle (see eqn 22d) and thus, $1-x$ to the Calvin-Benson cycle (see eqn 22e). The default value for x is 0.4, arising from $\varphi/(\varphi+3)$, where φ and 3 are ATP required for the CCM cycle and the Calvin-Benson cycle, respectively. For most C_4 species, $\varphi = 2$; so $x = 0.4$ (von Caemmerer & Furbank 1999). Thus, the RuBP regeneration-limited form of eqn 22e is expressed in terms of ATP supply. As with the C_3 model, it is metabolically important to keep ATP and NADPH in balance (Kramer & Evans 2011; Foyer et al. 2012); so, one may argue that ATP and NADPH co-determine the RuBP regeneration. For eqn 22e if NADPH supply is limiting, one can write, according to eqn 9a, that $x_1 = [1-f_{pseudo}/(1-f_{cyc})]J_2/4$, $x_2 = 2\gamma_*$, and $x_3 = 0$. Based on this NADPH-determined model, Yin & Struik (2012) stated that the photosynthetic quantum yield models for C_4 photosynthesis are the same as for C_3 photosynthesis, i.e. eqn 12a or eqn 12e, reflecting that there is no net NADPH requirement for the C_4 cycle (but see discussion later). Similarly, eqn 13a, eqn 13b and eqn 10b for calculating f_{cyc}, f_{pseudo} and ρ_2, respectively, also suit for C_4 photosynthesis.

As discussed earlier for C_3 photosynthesis, one can rely on the unique feature of the NADPH-dependent equation for quantum yield to infer possible values of f_{cyc} from measurements on quantum yields. Φ_{O2LL} of C_4 photosynthesis (virtually without photorespiration) is *ca* 0.069 (Björkman & Demmig1987), considerably lower than its counterpart value of C_3 photosynthesis in the absence of photorespiration. Using eqn 13a, Yin & Struik (2012) solved f_{cyc}, which was *ca* 0.45, considerably higher than the f_{cyc} of C_3

photosynthesis. This suggests that CET is essential for C_4 photosynthesis, required for generating ATP required for the operation of the CCM cycle.

Once f_{cyc} is known, ρ_2 can be calculated from eqn 10b. The obtained ρ_2 is *ca* 0.4 (Yin & Struik 2012). This differs from eqn 4, where the energy partitioning factor of 0.5 is also used for C_4 photosynthesis (von Caemmerer & Furbank 1999; von Caemmerer 2000, 2003). When f_{cyc} is known, f_{pseudo} can also be estimated from the assimilatory quotient (see eqn 13b) and is *ca* 0.07 (Yin & Struik 2012).

The equation equivalent to eqn 8 for C_3 photosynthesis, for the fraction of LET that keeps NADPH and ATP balance as required by C_4 metabolism, can be formulated as (see Yin & Struik 2012 for its derivation):

$$1 - f_{cyc} - f_{pseudo} = \frac{(4C_c+8\gamma_* O_c)(2+f_Q-f_{cyc})(1-x)}{h(3C_c+7\gamma_* O_c)(1+x\phi_L)} \quad (23a)$$

where ϕ_L is leakiness ($0 \le \phi_L \le 1$). Compared with eqn 8, eqn 23a has an extra facor $(1-x)/(1+x\phi_L)$. This suggests that compared with C_3 photosynthesis, the LET of C_4 photosynthesis is decreased at least by this factor to accommodate the required increase in CET. One can solve eqn 23a for leakiness:

$$\phi_L = \frac{(4C_c+8\gamma_* O_c)(2+f_Q-f_{cyc})(1-x)}{h(3C_c+7\gamma_* O_c)(1-f_{cyc}-f_{pseudo})x} - \frac{1}{x} \quad (23b)$$

Given the above indicative values of f_{cyc} and f_{pseudo} based on quantum yield data, one can use eqn 23b to explore likely values of uncertain parameters f_Q and h that can give a realistic estimate of leakiness. Using either obligatory or no operation of the Q cycle (f_Q = 1 or 0) and three likely values of h (3, 4 and 4.67, see earlier), Yin & Struik (2012) showed that only the combination that f_Q = 1 and h = 4 can give a realistic value of ϕ_L (Fig. 7). The obligatory Q cycle has long been recognised for C_4 photosynthesis (Furbank et al. 1990). But whether the H^+:ATP ratio (h) is 3, 4 or 4.67 is uncertain. The model results shown in Fig. 7 support thermodynamic experiments (Steigmiller et al. 2008; Peterson et al. 2012) showing that h is 4.

The model discussed so far, for both C_3 and C_4 photosynthesis, assumes that CET, when combined with the Q cycle, generates two H^+ per electron (Fig. 2). However, CET may follow the NAD(P)H dehydrogenase (NDH)-dependent pathway (Yamori et al. 2011; Ishikawa et al. 2016; Strand et al. 2017). When this pathway is operating, CET generates four H^+ per electron and Karmer and Evans (2011) indicated that very likely this pathway is active in C_4 plants. Let f_{NDH} be the fraction of CET that follows the NDH-dependent pathway. Then the ATP production factor z as in eqn 9e for such a case is (Yin & Struik 2021):

$$z = \frac{2+f_Q-f_{cyc}(1-2f_{NDH})}{h(1-f_{cyc})} \quad (24a)$$

Eqn 24a becomes eqn 9e if $f_{NDH} = 0$. Again, the uncertainty with regard to the value of f_{NDH} has no impact on the model for the NADPH-dependent quantum yield, so the above estimation of f_{cyc} using the NADPH-dependent quantum yield model is still valid. Yin & Struik (2012) showed that this highly efficient H^+-translocating pathway of CET can't be obligatory as this would result in unrealistic high estimates of leakiness. Here we try to assess the extent to which CET should be this highly efficient pathway if h is 4.67 (=14/3, Seelert et al. 2000; again recently, Hahn et al. 2018). This can be achieved by equating eqn 24a with h =14/3 to eqn 9e with $h = 4$, and then solving for f_{NDH}:

$$f_{NDH} = \frac{2+f_Q-f_{cyc}}{12f_{cyc}} \quad (24b)$$

This gives that f_{NDH} is *ca* 0.47 if $f_Q = 1$ and $f_{cyc} = 0.45$, meaning that about half of the total CET have to follow this highly efficient pathway in order to meet the high ATP requirement in C_4 photosynthesis, if the H^+ requirement per ATP synthesis is as high as 4.67. This suggests a method to estimate f_{NDH}, as this parameter has been estimated only by trial and error (Bellasio & Farquhar 2019).

Combining $h = 4$ and $f_{NDH} = 0$ or $h = 4.67$ and $f_{NDH} = 0.47$ suggests that the ATP production factor per PSII electron transport (z) is *ca* 1.16. This differs from the standard C_4 model of von Caemmerer & Furbank (1999), in which J_{atp} is set to equal PSII electron

transport rate. The standard model assumes: (i) the absence of CET and (ii) and $h = 3$. Eqn 9e suggests that these assumptions combined with an obligatory Q cycle make $z = 1$.

Accommodating the C_4 species mixed with PEP-CK

It is important to point out that the above results of energetics are valid only for NADP-ME or NAD-ME subtypes of C_4 photosynthesis, although the standard model has been wrongly applied in some reports to the PEP-CK subtype. As stated earlier, the value of 0.4 for x stems from that the parameter φ in eqn 22d is 2, referring to two mol ATP required per CCM cycle for regenerating PEP by pyruvate phosphate dikinase (PPDK) in the M cell (Hatch 1987; Kanai & Edwards 1999). This high ATP requirement is reflected in measured quantum yields in species of the malic-enzyme subtypes, from which the model derived f_{cyc} was high (*ca* 0.45). In the PEP-CK subtype, however, part of the oxaloacetate produced by the initial PEP carboxylation step moves to and is decarboxylated in the BS cytosol by PEP-CK (Hatch 1987). This decarboxylation reaction also generates PEP (requiring only one molecule of ATP per reaction), thereby partly bypassing the expensive step of PEP regeneration by PPDK. The remaining oxaloacetates are reduced to malate in the M cells, which move to and are decarboxylated in BS mitochondria. This decarboxylation also releases NADH, which drives mitochondrial electron transport to provide ATP for fuelling PEP-CK possibly (Kanai & Edwards 1999), thereby further decreasing the chloroplastic ATP requirement. Given that the pure PEP-CK type hardly exists in nature and species having PEP-CK are often mixed with other decarboxylation types (Furbank 2011; Wang et al. 2014), Yin & Struik (2021) presented a model for the electron transport-limited rate in all C_4 subtypes including their mixed types.

In this model, eqns 22a-e still apply, but with:

$$x_1 = \left(1 - \frac{f_{\mathrm{pseudo}}}{1 - f_{\mathrm{cyc}}}\right) \frac{J_2}{4 + 2a} \tag{25a}$$

and x_2 and x_3 are as defined earlier (i.e., $x_2 = 2\gamma^*$, and $x_3 = 0$). In eqn 25a, parameter a is the fraction of oxaloacetates that are reduced, using NADPH (equivalent to 2 electrons) from M chloroplasts, to malate moving to the BS mitochondria. To accommodate various C_4 types, two further adjustments are needed. Firstly, the chloroplastic ATP requirement for the CCM cycle (φ) should be changed from 2 for the malic-enzyme subtypes to:

$$\varphi = 2 - (n + 1)a \tag{25b}$$

where n is the number of ATP produced per NADH oxidation from mitochondrial electron transport (n = 2.5~3.0; Taiz & Zeiger 2002), the coefficient 1 represents one molecule ATP fewer required for per PEP regenerated by PEP-CK than by PPDK, and so, the term $(n + 1)a$ represents ATP saved from engaging the PEP-CK mechanism, relative to the malic-enzyme mechanisms (Yin & Struik 2021). Secondly, for the types involving PEP-CK, x is changed to:

$$x = \frac{2-(n+1)a}{5-(n+1)a} \tag{25c}$$

These equations have taken into account the required balance of NH_2-groups between M and BS cells. The analysis of Yin & Struik (2021) suggested that $0 \le a \le 0.36$~0.40, and if $a = 0$, the model returns to the equations discussed earlier for the malic-enzyme subtypes. The model predicts that the additional cost with a mol NADPH requirement per mol CO_2 assimilated is overcompensated by the decreased chloroplastic ATP requirement for the CCM cycle, thereby predicting a higher Φ_{CO2} in species involving the PEP-CK activity. However, the observed little advantage in Φ_{CO2} of the PEP-CK over the NADP-ME species (Ehleringer & Pearcy 1983) suggests the need of more studies to understand whether the energetic advantages are cancelled out by leakiness in the PEP-CK types.

Conclusions and remarks

The FvCB model has been proven successful in most cases in fitting response curves for predicting photosynthetic rates (e.g. Kumarathunge et al. 2019). The model extensions

reviewed here are hardly meant to replace the canonical FvCB model for that, but more to provide tools for analysing uncertainties and better understanding underlying physiology of photosynthesis. From our review in this context, we can make the following summary points:

(1) Relative to the ATP-determined form, the extended NADPH-determined form for electron transport-limited rate has fewer uncertain parameters and is yet related to the fraction for CET (f_{cyc}). This singular feature of the model allows f_{cyc} to be first estimated from easily measured quantum yield for photosynthesis and quantum yield for photosystem electron transport. The estimated f_{cyc} is negligible (*ca* 0.06) for C_3 photosynthesis vs *ca* 0.45-0.50 for malic-enzyme subtypes of C_4 photosynthesis. The NADPH-determined form also has an advantage in modelling C_4 photosynthesis involving decarboxylation by PEP-CK, which requires additional NADPH, a lower ATP:NADPH ratio and probably a lower f_{cyc}, than the malic-enzyme subtypes.

(2) Because of such a difference in f_{cyc}, the factor for excitation partitioning to PSII (ρ_2) was *ca* 0.5 or slightly higher for C_3 photosynthesis, but *ca* 0.4 for malic-enzyme subtypes of C_4 photosynthesis. This differs from the canonical FvCB model where 0.5 is always set for both C_3 and C_4 photosynthesis models.

(3) If f_{cyc} is known, one can also estimate f_{pseuso} based on the assimilatory quotient (see eqn 13b), and futher infer values for uncertain parameters f_Q and h in view of the ATP:NADPH ratio as required by metabolism. The most likely values are: $f_Q = 1$ combined with $h = 4$ for C_4 plants, and with $h = 4.00$ or 4.67 for C_3 plants. If h is 4.67 for C_4 plants, then *ca* 50% of CET must follow the NDH-dependent pathway in the malic-enzyme subtypes of C_4 plants. The stoichiometric coefficients ($f_Q = 0$ and $h = 3$) assumed in the ATP-limited form of the canonical C_3 model (eqn 3b) and of the standard C_4 model are obsolete.

(4) The TPU limitation is commonly ignored in modelling C_4 photosynthesis probably because it is hard to identify this limitation from its A-C_i curves. While the extension of the

canonical FvCB model to account for this limitation to C_3 photosynthesis in relation to the glycine export from the photorespiratory pathway has long been made, it appears now that assuming serine (rather than glycine) to exit from the pathway is more likely and internally consistent with regard to the CO_2 compensation point. However, this notion may change as we find out more about the nature of carbon export as CH_2-THF.

(5) Under TPU limited conditions plants can increase CO_2 uptake, by serine, glycine, or CH_2-THF exit from the photorespiratory pathway and associated *de novo* nitrogen assimilation or C_1 metabolism in leaves of C_3 plants. However, there exists nitrogen assimilation not associated with the photorespiratory pathway, especially for low-photorespiration situations as occurring in C_4 plants or in C_3 plants under high CO_2/low O_2 conditions.

(6) Loss as a result of photorespiration in C_3 plants is lower than the commonly suggested value, owing to: (i) glycine, serine and CH_2-THF exports, and (ii) significant refixation of (photo)respired CO_2 both within mesophyll cells and via IAS. On the other hand, (photo)respired CO_2 release decreases the chance of CO_2 coming from IAS being assimilated. It is this net refixation of the (photo)respired CO_2 that is taken into account by the coupled CO_2-diffusion and FvCB model.

This review did not discuss the C_3-C_4 intermediate photosynthesis, for which von Caemmerer (2000) outlined a modelling framework. We also hardly discussed modelling photosynthetic temperature response (see Bernacchi et al. 2013), but focused on photosynthetic CO_2- and light-responses. One may be surprised to notice that eqns 4 and 11 for modelling the light-response of electron transport are still empirical. However, Farquhar & von Caemmerer (1981) presented some mechanistic basis for using these simple equations. Harbinson & Yin (2017) reported a mechanistic but more complex equation for the irradiance response of PSI electron transport rate. The essence of the FvCB model is its simplicity while

capturing the most important contributing mechanisms of photosynthesis (Farquhar et al. 2001). This feature is maintained in the extended models as all the equations we reviewed are analytical, and users can easily implement them for thought experiments to explore changes of photosynthetic pathways. The simplicity means that the models are for steady-state photosynthesis. Excellent, more detailed models for photosynthesis under either steady-state or fluctuating conditions and for the photosynthetic acclimation to growth environment are all omitted in this review, despite their high relevance for photosynthesis in field environments.

References

Abadie, C., & Tcherkez, G. (2019). *In vivo* phospho*enol*pyruvate carboxylase activity is controlled by CO_2 and O_2 mole fractions and represents a major flux at high photorespiration rates. *New Phytologist*, 221, 1843-1852.

Abadie, C., Boex-Fontvieille, E.R.A., Carroll, A.J., & Tcherkez, G. (2016). *In vivo* stoichiometry of photorespiratory metabolism. *Nature Plants*, 2, DOI 10.1038/NPLANTS.2015.220.

Abadie, C., Bathellier, C., & Tcherkez, G. (2018). Carbon allocation to major metabolites in illuminated leaves is not just proportional to photosynthesis when gaseous conditions (CO_2 and O_2) vary. *New Phytologist*, 218, 94-106.

Allen, J.F. (2003). Cyclic, pseudocyclic and noncyclic photophosphorylation: new links in the chain. *Trends in Plant Science*, 8, 15-19.

Alonso-Cantabrana, H., Cousins, A.B., Danila, F., Ryan, T., Sharwood, R.E., von Caemmerer, S., & Furbank, R.T. (2018). Diffusion of CO_2 across the mesophyll-bundle sheath cell interface in a C_4 plant with genetically reduced PEP carboxylase activity. *Plant Physiology*, 178, 72-81.

Asada, K. (1999). The water-water cycle in chloroplasts: Scavenging of active oxygens and dissipation of excess photons. *Annual Review of Plant Physiology and Plant Molecular Biology*, 50, 601-639.

Avenson, T.J., Kanazawa, A., Cruz, J.A., Takizawa, K., Ettinger, W.E., & Kramer, D.M. (2005). Integrating the proton circuit into photosynthesis: progress and challenges. *Plant, Cell & Environment*, 28, 97-109.

Bagley, J., Rosenthal, D.M., Ruiz-Vera, U.M., Siebers, M.H., Kumar, P., Ort, D.R., & Bernacchi, C.J. (2015). The influence of photosynthetic acclimation to rising CO_2 and warmer temperatures on leaf and canopy photosynthesis models. *Global Biogeochemical Cycles*, 29(2), 194-206.

Baker, N.R., Harbinson, J., & Kramer, D.M. (2007). Determining the limitations and regulation of photosynthetic energy transduction in leaves. *Plant, Cell & Environment*, 30, 1107-1125.

Barbour, M.M., Evans, J.R., Simonin, K.A., & von Caemmerer, S. (2016). Online CO_2 and H_2O oxygen isotope fractionation allows estimation of mesophyll conductance in C_4 plants, and reveals that mesophyll conductance decreases as leaves age in both C_4 and C_3 plants. *New Phytologist*, 210, 875-889.

Bellasio, C., & Griffiths, H. (2014). Acclimation to low light by C_4 maize: implications for bundle sheath leakiness. *Plant, Cell & Environment* 37, 1046-1058.

Bellasio, C., Farquhar, G.D. (2019). A leaf-level biochemical model simulating the introduction of C_2 and C_4 photosynthesis in C_3 rice: gains, losses and metabolite fluxes. *New Phytologist*, 223, 150-166.

Bernacchi, C.J., Portis, A.R., Nakano, H., von Caemmerer, S., & Long, S.P. (2002). Temperature response of mesophyll conductance. Implication for the determination of Rubisco enzyme kinetics and for limitations to photosynthesis *in vivo*. *Plant Physiology*, 130, 1992-1998.

Bernacchi, C.J., Bagley, J.E., Serbin, S.P., Ruiz-Vera, U.M., Rosenthal, D.M., & Vanloocke, A. (2013). Modelling C_3 photosynthesis from the chloroplast to the ecosystem. *Plant, Cell & Environment*, 36, 1641-1657.

Berry, J.A., & Farquhar, G.D. (1978). The CO_2-concentrating function of C_4 photosynthesis. A biochemical model. In *Proceedings of the 4th International Congress on Photosynthesis* (eds D.O. Hall, J. Coombs & T.W. Goodwin). pp. 119-131. London: Biochemical Society.

Björkman, O., & Demmig, B. (1987). Photon yield of O_2 evolution and chlorophyll fluorescence characteristics at 77 K among vascular plants of diverse origins. *Planta*, 170, 489-504.

Bloom, A.J. (2015). Photorespiration and nitrate assimilation: a major intersection between plant carbon and nitrogen. *Photosynthesis Research*, 123, 117-128.

Bloom, A.J., Caldwell, R.M., Finazzo, J., Warner, R.L., & Weissbart, J. (1989). Oxygen and carbon dioxide fluxes from barley shoots depend on nitrate assimilation. *Plant Physiology*, 91, 352-356.

Boyd, R.A., Gandin, A., & Cousins, A.B. (2015). Temperature response of C_4 photosynthesis: Biochemical analysis of Rubisco, phospho*enol*pyruvate carboxylase and carbonic anhydrase in *Setaria viridis*. *Plant Physiology*, 169, 1850-1861.

Busch, F.A. (2020). Photorespiration in the context of Rubisco biochemistry, CO_2 diffusion and metabolism. *The Plant Journal*, 101, 919-939.

Busch, F.A., & Sage, R.F. (2017). The sensitivity of photosynthesis to O_2 and CO_2 concentration identifies strong Rubisco control above the thermal optimum. *New Phytologist*, 213, 1036-1051.

Busch, F.A., Sage, T.L., Cousins, A.B., & Sage, R.F., 2013. C_3 plants enhance rates of photosynthesis by reassimilating photorespired and respired CO_2. *Plant, Cell & Environment*, 36, 200-212.

Busch, F.A., Sage, R.F., & Farquhar, G.D. (2018). Plants increases CO_2 uptake by assimilating nitrogen via the photorespiratory pathway. *Nature Plants*, 4, 46-54.

Busch, F.A., Holloway-Phillips, M., Stuart-Williams, H., & Farquhar, G.D. (2020). Revisiting carbon isotope discrimination in C_3 plants shows respiration rules when photosynthesis is low. *Nature Plants*, 6, 245-258. doi: 10.1038/s41477-020-0606-6.

Cornic, G., Bukhov, N.G., Wiese, C., Bligny, R., & Heber, U. (2000). Flexible coupling between light-dependent electron and vectorial proton transport in illuminated leaves of C_3 plants. Role of photosystem I-dependent proton pumping. *Planta*, 210, 468-477.

Cousins, A.B., Ghannoum, O., von Caemmerer, S., & Badger, M.R. (2010). Simultaneous determination of Rubisco carboxylase and oxygenase kinetic parameters in *Triticum aestivum* and *Zea mays* using membrane inlet mass spectrometry. *Plant, Cell & Environment*, 33, 444-452.

Danila, F.R., Thakur, V., Chatterjee, J., Bala, S., Coe, R.A., Acebron, K., Furbank, R.T., von Caemmerer, S., & Quick, W.P. (2021). Bundle sheath suberisation is required for C_4 photosynthesis in a *Setaria viridis* mutant. *Communication Biology*, 4: 254|doi: 10.1038/s42003-021-01772-4.

Deans, R.M., Farquhar, G.D., & Busch, F.A. (2019). Estimating stomatal and biochemical limitations during photosynthetic induction. *Plant, Cell & Environment*, 42, 3227-3240.

Deans, R.M., Brodribb T.J,, Busch, F.A., & Farquhar, G.D. (2020). Optimization can provide the fundamental link between leaf photosynthesis, gas exchange and water relations. *Nature Plants*, 6, 1116-1125.

Dingkuhn, M., Luquet, D., Fabre, D., Muller, M., Yin, X., & Paul, M. (2020). The case for improving crop carbon sink strength or plasticity for a CO_2-rich future. *Current Opinion in Plant Biology*, 56, 259-272.

Ehleringer, J., & Pearcy, R.W. (1983). Variation in quantum yield for CO_2 uptake among C_3 and C_4 plants. *Plant Physiology*, 73, 555-559.

Eichelmann, H., Oja, V., Peterson, R.B., & Laisk, A. (2011). The rate of nitrite reduction in leaves as indicated by O_2 and CO_2 exchange during photosynthesis. *Journal of Experimental Botany*, 62, 2205-2215.

Ellsworth, D.S., Crous, K.Y., Lambers, H., & Cooke, J. (2015). Phosphorus recycling in photorespiration maintains high photosynthetic capacity in woody species. *Plant, Cell & Environment*, 38, 1142-1156.

Ethier, G.J., & Livingston, N.J. (2004). On the need to incorporate sensitivity to CO2 transfer conductance into the Farquhar-von Caemmerer-Berry leaf photosynthesis model. *Plant, Cell & Environment*, 27, 137-153.

Evans, J.R. (1987). The dependence of quantum yield on wavelength and growth irradiance. *Australian Journal of Plant Physiology*, 14, 69-79.

Evans, J.R. (2021). Mesophyll conductance: walls, membranes and spatial complexity. *New Phytologist*, 229, 1864-1876.

Evans, J.R., Sharkey, T.D., Berry, J.A., & Farquhar, G.D. (1986). Carbon isotope discrimination measured concurrently with gas-exchange to investigate CO_2 diffusion in leaves of higher plants. *Australian Journal of Plant Physiology* 13, 281-292.

Evans, J.R., von Caemmerer, S., Setchell, B.A., & Hudson, G.S., 1994. The relationship between CO_2 transfer conductance and leaf anatomy in transgenic tobacco with a reduced content of Rubisco. *Australian Journal of Plant Physiology*, 21, 475-495.

Fabre, D., Yin, X., Dingkuhn, M., Clément-Vidal, A., Roques, S., Lauriane, R., Soutiras, A., & Luquet, D. (2019). Is triose phosphate utilization involved in the feedback inhibition of photosynthesis in rice under conditions of sink limitation? *Journal of Experimental Botany*, 70, 5773-5785.

Fabre, D., Dingkuhn, M., Yin, X., Clément-Vidal, A., Roques, S., Soutiras, A., & Luquet, D. (2020). Genotypic variation in source and sink traits affects the response of photosynthesis and growth to elevated atmospheric CO_2. *Plant, Cell & Environment*, 43, 579-593.

Farquhar, G.D. (1983). On the nature of carbon isotope discrimination in C_4 species. *Australian Journal of Plant Physiology*, 10: 205-226.

Farquhar G.D., & von Caemmerer, S. (1981). Electron transport limitations in the CO_2 assimilation rate of leaves: A model and some observations in *Phaseolus vulgaris* L. In *Photosynthesis, Vol. IV: Regulation of Carbon Metabolism* (ed. G. Akoyunoglou), pp.163-175. Balaban International Science Services, Philadelphia, USA.

Farquhar, G.D., & von Caemmerer, S. (1982). Modelling of photosynthetic response to environmental conditions. In: O.L. Lange, P.S. Nobel, C.B. Osmond and H. Ziegler (editors) Physiological Plant Ecology II, Water relations and carbon assimilation. Encyclopaedia of Plant Physiology, New Series, Vol. 12 B, Springer Verlag, Berlin, p. 549-588.

Farquhar, G.D., von Caemmerer, S., & Berry, J.A. (1980). A biochemical model of photosynthetic CO_2 assimilation in leaves of C_3 species. *Planta*, 149: 78-90.

Farquhar, G.D., von Caemmerer, S., & Berry, J.A. (2001) Models of photosynthesis. *Plant Physiology*, 125: 42-45.

Farquhar, G.D., & Wong, S.C. (1984). An empirical model of stomatal conductance. *Australian Journal of Plant Physiology*, 11, 191-210.

Farquhar, G.D., O'Leary, M.H., & Berry, J.A. (1982). On the relationship between carbon isotope discrimination and the intercellular carbon dioxide concentration in leaves. *Australian Journal of Plant Physiology*, 9, 121-137.

Flexas, J., Diaz-Espejo, A., Galmes, J., Kaldenhoff, R., Medrano, H., & Ribas-Carbó, M. (2007). Rapid variation of mesophyll conductance in response to changes in CO_2 concentration around leaves. *Plant, Cell & Environment*, 30, 1284-1298.

Foyer, C.H., Neukermans, J., Queval, G., Noctor, G., & Harbinson, J., (2012). Photosynthetic control of electron transport and the regulation of gene expression. *Journal of Experimental Botany*, 63, 1637-1661.

Furbank, R.T. (2011). Evolution of the C_4 photosynthetic mechanism: are there really three C_4 acid decarboxylation types? *Journal of Experimental Botany*, 62, 3103-3208.

Furbank, R.T., Jenkins, C.L.D., & Hatch, M.D., (1990). C_4 photosynthesis: Quantum requirement, C_4 acid overcycling and Q-cycle involvement. *Australian Journal of Plant Physiology*, 17, 1-7.

Genty, B., & Harbinson, J. (1996). Regulation of light utilization for photosynthetic electron transport. P. 67-99. *In* N.R. Baker (editor) Photosynthesis and the Environment. Vol 5 book series 'Advances in Photosynthesis and Respiration'. Kluwer Academic Publishers, The Netherlands.

Ghannoum, O., Evans, J.R., Chow, W.S., Andrews, J., Conroy, J., & von Caemmerer, S. (2005). Faster Rubisco is the key to superior nitrogen-use efficiency in NADP-malic enzyme relative to NAD-malic enzyme C_4 grasses. *Plant Physiology*, 137, 638-650.

Gu, L., Pallardy, S.D., Tu, K., Law, B.E., & Wullschleger, S.D. (2010). Reliable estimation of biochemical parameters from C_3 leaf photosynthesis-intercellular carbon dioxide response curves. *Plant, Cell & Environment*, 33, 1852-1874.

Gu, L., & Sun, Y. (2014). Artefactual responses of mesophyll conductance to CO_2 and irradiance estimated with the variable J and online isotope discrimination methods. *Plant, Cell & Environment*, 37, 1231-1249.

Hahn, A,, Vonck, J., Mills, D.J., Meier, T., & Kühlbrandt, W. (2018). Structure, mechanism, and regulation of the chloroplast ATP synthase. *Science*, 360, eaat4318 doi:10.1126/science.aat4318.

Hatch, M.D., 1987. C_4 photosynthesis: a unique blend of modified biochemistry, anatomy and ultrastructure. Biochimica et Biophysica Acta 895: 81-106.

Harbinson, J., & Yin, X. (2017). A model for the irradiance responses of photosynthesis. *Physiologia Plantarum*, 161, 109-123.

Harley, P.C., & Sharkey, T.D. (1991). An improved model of C_3 photosynthesis at high CO_2: Reversed O_2 sensitivity explained by lack of glycerate reentry into the chloroplast. *Photosynthesis Research*, 27, 169-178.

Harley, P.C., Loreto, F., Di Marco, G., & Sharkey, T.D. (1992). Theoretical considerations when estimating the mesophyll conductance to CO_2 flux by analysis of the response of photosynthesis to CO_2. *Plant Physiology*, 98, 1429-1436.

He, D., & Edwards, G.E. (1996). Estimation of diffusive resistance of bundle sheath cells to CO_2 from modeling of C_4 photosynthesis. *Photosynthesis Research*, 49, 195-208.

Hogewoning, S.W., Wientjes, E., Douwstra, P., Trouwborst, G., van Ieperen, W., Croce, R., & Harbinson, J. (2012). Photosynthetic quantum yield dynamics: From photosystems to leaves. *The Plant Cell*, 24, 1921-1935.

Ishikawa, N., Takabayashi, A., Noguchi, K., Tazoe, Y., Yamamoto, H., von Caemmerer, S., Sato, F., & Endo, T. (2016). NDH-mediated cyclic electron flow around photosystem I is crucial for C_4 photosynthesis. *Plant & Cell Physiology*, 57, 2020-2028

Kaschuk, G., Yin, X., Hungria, M, Leffelaar, P.A., Giller, K.E., & Kuyper, T.W. (2012). Photosynthetic adaptation of soybean due to varying effectiveness of N_2 fixation by two distinct *Bradyrhizobium japonicum* strains. *Environmental and Experimental Botany*, 76, 1-6.

Kebeish, R., Niessen, M., Thirshnaveni, K., Bari, R., Hirsch, H.-J., Rosenkranz, R., Stäbler, N., Schönfeld, B., Kreuzaler, F., & Peterhänsel, C. (2007). Chloroplastic photorespiratory bypass increases photosynthesis and biomass production in *Arabidopsis thaliana*. *Nature Biotechnology*, 25, 593-599.

Kanai, R., & Edwards, G.E. (1999). The biochemistry of the C_4 photosynthesis. P. 49-87. In: R.F. Sage and R.K. Monson (eds) C_4 Plant Biology. Academic Press, Toronto.

Kiirats, O., Lea, P.J., Franceschi, V.R., & Edwards, G.E. (2002). Bundle sheath diffusive resistance to CO_2 and effectiveness of C_4 photosynthesis and refixation of photorespired CO_2 in a C_4 cycle mutant and wild-type *Amaranthus edulis*. *Plant Physiology*, 130, 964-976 (with Corrections in Plant Physiology 132, 400).

Kramer, D.M., & Evans, J.R. (2011). The importance of energy balance in improving photosynthetic productivity. *Plant Physiology*, 155, 70-78.

Kromdijk, J., Griffiths, H., & Schepers, H.E. (2010). Can the progressive increase of C_4 bundle sheath leakiness at low PFD be explained by incomplete suppression of photorespiration? *Plant, Cell & Environment*, 33, 1935-1948.

Kumarathunge, D.P., Medlyn, B.E., Drake, J.E., Rogers, A., & Tjoelker, M.G. (2019). No evidence for triose phosphate limitation of light saturated leaf photosynthesis under current atmospheric CO_2 concentration. *Plant, Cell & Environment*, 42, 3241-3252..

Laing, W.A., Ogren, W.L., & Hageman, R.H. (1974). Regulation of soybean net photosynthetic CO_2 fixation by the interaction of CO_2, O_2, and ribulose 1,5-diphosphate carboxylase. *Plant Physiology*, 54, 678-685.

Leuning, R. (1990). Modelling stomatal behaviour and photosynthesis of *Eucalyptus grandis*. *Australian Journal of Plant Physiology*, 17, 159-175.

Lim, S.-L., Voon, C.P., Guan, X., Yang, Y., Gardestrom, P., & Lim, B.L. (2020). *In Planta* study of photosynthesis and photorespiration using NADPH and NADH/NAD^+ fluorescent protein sensors. *Nature Communications*, 11, 3238 (https://doi.org/10.1038/s41467-020-17056-0).

Long, S.P., & Bernacchi, C.J. (2003). Gas exchange measurements, what can they tell us about the underlying limitations to photosynthesis? Procedures and sources of error. *Journal of Experimental Botany*, 54, 2393-2401.

Long, S.P., Postl, W.F., & Bolhár-Nordenkampf, H.R. (1993). Quantum yields for uptake of carbon dioxide in C_3 vascular plants of contrasting habitats and taxonomic groupings. *Planta,* 189, 226-234.

McClain, A.L., & Sharkey, T.D. (2019). Triose phosphate utilization and beyond: from photosynthesis to end product synthesis. *Journal of Experimental Botany*, 70, 1755-1766.

Noctor, G., & Foyer, C.H. (1998). A re-evaluation of the ATP:NADPH budget during C_3 photosynthesis: a contribution from nitrate assimilation and its associated respiratory activity? *Journal of Experimental Botany*, 49, 1895-1908.

Ort, D.R., & Baker, N.R. (2002). A photoprotective role for O_2 as an alternative electron sink in photosynthesis? *Current Opinion in Plant Biology*, 5, 193-198.

Pammenter, N.W., Loreto, F., & Sharkey, T.D., 1993. End product feedback effects on photosynthetic electron transport. *Photosynthesis Research*, 35, 5-14.

Peterhansel, C., Blume, C., & Offermann, S. (2013). Photorespiratory bypasses: how can they work? *Journal of Experimental Botany*, 64, 709-715.

Petersen, J., Förster, K., Turina, P., & Gräber, P. (2012). Comparison of the H^+/ATP ratios of the H^+-ATPsynthases from yeast and from chloroplast. *Proceedings of the National Academy of Sciences of the United States of America*, 109, 11150-11155.

Pitman, A.J. (2003). The evolution of, and revolution in, land surface schemes designed for climate models. *International Journal of Climatology*, 23(5), 479-510.

Pons, T.L., Flexas, J., von Caemmerer, S., Evans, J.R., Genty, B., Ribas-Carbo, M., & Brugnoli, E. (2009). Estimating mesophyll conductance to CO_2: Methodology, potential errors, and recommendations. *Journal of Experimental Botany*, 60, 2217-2234.

Rogers, A., Medlyn, B.E., & Dukes, J.S. (2014). Improving representation of photosynthesis in Earth System Models. *New Phytologist*, 204(1), 12-14.

Ros, R., Muñoz-Bertomeu, J., & Krueger, S. (2014). Serine in plants: biosynthesis, metabolism, and functions. *Trends in Plant Science*, 19, 564-569.

Sacksteder, C.A., Kanazawa, A., Jacoby, M.E., & Kramer, D.M. (2000). The proton to electron stoichiometry of steady-state photosynthesis in living plants: A proton-pumping Q cycle is continuously engaged. *Proceedings of the National Academy of Sciences of USA*, 97, 14283-14288.

Seelert, H., Poetsch, A., Dencher, N.A., Engel, A., Stahlberg, H., & Müller, D.J. (2000). Proton powered turbine of a plant motor. *Nature*, 405, 418-419.

Sage, T.L., & Sage, R.F. (2009). The functional anatomy of rice leaves: Implications for refixation of photorespiratory CO_2 and efforts to engineer C_4 photosynthesis into rice. *Plant & Cell Physiology*, 50, 756-772.

Sellers, P.J., Randall, D.A., Collatz, G.J., Berry, J.A., Field, C.B., Dazlich, D.A., Zhang, C., Collelo, G.D. & Bounoua, L. (1996). A revised land surface parameterization (SiB2) for atmospheric GCMS. Part I: model formulation. *Journal of Climate*, 9(4), 676-705.

Sharkey, T.D. (1985a). O_2-insensitive photosynthesis in C_3 plants: Its occurrence and a possible explanation. *Plant Physiology*, 78, 71-75.

Sharkey, T.D. (1985b). Photosynthesis in intact leaves of C_3 plants: Physics, physiology and rate limitations. *The Botanical Review*, 51, 53-105.

Sharkey, T.D., 2019. Is triose phosphate utilization important for understanding photosynthesis? Journal of Experimental Botany 70: 5521-5525.

Sharkey, T.D., & Vassey, T.L. (1989). Low oxygen inhibition of photosynthesis is caused by inhibition of starch synthesis. *Plant Physiology*, 90, 385-387.

Sharkey, T.D., Bernacchi, C.J., Farquhar, G.D., & Singsaas, E.L. (2007). Fitting photosynthetic carbon dioxide response curves for C_3 leaves. *Plant, Cell & Environment*, 30: 1035-1040.

Sharwood, R., Ghannoum, O., Kapralov, M.V. Gunn, L.H., & Whitney, S.M. (2016). Temperature responses of Rubisco from Paniceae grasses provide opportunities for improving C_3 photosynthesis. *Nature Plants*, 2, 16186. https://doi.org/10.1038/nplants.2016.186.

Shen, B., Wang, L., Lin, X., Yao, Z., Xu, H., Zhu, C., Teng, H., Cui, L., Zhang, J., He, Z., & Peng, X., (2019). Engineering a new chloroplastic photorespiratory bypass to increase photosynthetic efficiency and productivity in rice. *Molecular Plants*, 12,199-214.

Skillman, J.B. (2008). Quantum yield variation across the three pathways of photosynthesis: not yet out of the dark. *Journal of Experimental Botany*, 59, 1647-1661.

South, P.F., Cavanagh, A.P., Liu, H.W., & Ort, D.R. (2019). Synthetic glycolate metabolism pathways stimulate crop growth and productivity in the field. *Science*, 363, Issue 6422, eaat9077.

Steigmiller, S., Turina, P., & Gräber, P. (2008). The thermodynamic H^+/ATP ratios of the H^+-ATPsynthases from the chloroplasts and *Escherichia coli*. *Proceedings of the National Academy of Sciences of the United States of America*, 105, 3745-3750.

Strand, D.D., Fisher, N., & Kramer, D.M. (2017). The higher plant plastid NAD(P)H dehydrogenase-like complex (NDH) is a high efficiency proton pump that increases ATP production by cyclic electron flow. *Journal of Biological Chemistry*, 292, 11850-11860.

Taiz, L., & Zeiger, E. (2002). Plant Physiology (3rd ed). 690 pp. Sunderland: Sinauer Associates.

Tcherkez, G. and Limami, A.N., 2019. Net photosynthetic CO_2 assimilation: more than just CO_2 and O_2 reduction cycles. New Phytologist 223: 520-529.

Tcherkez, G., Gauthier, P., Buckley, T.N., et al., (2017). Leaf day respiration: low CO_2 flux but high significance for metabolism and carbon balance. *New Phytologist*, 216, 986-1001.

Tholen, D., Ethier, G., Genty, B., Pepin, S., & Zhu, X.-G. (2012). Variable mesophyll conductance revisited: theoretical background and experimental implications. *Plant, Cell & Environment*, 35, 2087-2103.

Ubierna, N., Sun, W., Kramer, D.M., & Cousins, A.B. (2013). The efficiency of C_4 photosynthesis under low light conditions in *Zea mays*, *Miscanthus × giganteus* and *Flaveria bidentis*. *Plant, Cell & Environment*, 36, 365-381.

Ubierna, N., Cernusak, L.A., Holloway-Phillips, M., Busch, F.A., Cousins, A.B., & Farquhar, G.D. (2019). Critical review: incorporating the arrangement of mitochondria and chloroplasts into models of photosynthesis and carbon isotope discrimination. *Photosynthesis Research*, 141, 5-31.

van der Putten, P.E.L., Yin, X., & Struik, P.C. (2018). Calibration matters: on the procedure of using the chlorophyll fluorescence method to estimate mesophyll conductance. *Journal of Plant Physiology*, 220, 167-172.

von Caemmerer, S. (2000). Biochemical models of leaf photosynthesis. CSIRO Publishing, Collingwood, Australia.

von Caemmerer, S. (2013). Steady-state models of photosynthesis. *Plant, Cell & Environment*, 36, 1617-1630.

von Caemmerer, S., & Evans, J.R. (1991). Determination of the average partial pressure of CO_2 in chloroplasts from leaves of several C_3 plants. *Australian Journal of Plant Physiology*, 18, 287-305.

von Caemmerer, S., & Farquhar, G.D. (1981). Some relationships between the biochemistry of photosynthesis and the gas exchange of leaves. *Planta*, 153, 376-387.

von Caemmerer, S., & Furbank, R.T. (1999). Modeling C_4 photosynthesis. P. 173-211. In: R.F. Sage and R.K. Monson (eds) C_4 Plant Biology. Academic Press, Toronto.

von Caemmerer, S., Evans, J.R., Hudson, G.S., & Andrews, T.J. (1994). The kinetics of ribulose-1,5-bisphosphate carboxylase/oxygenase in vivo inferred from measurements of photosynthesis in leaves of transgenic tobacco. *Planta*, 195, 88-97.

Wang, Y., Brautigam, A., Weber, A.P.M., & Zhu, X.-G. (2014). Three distinct biochemical subtypes of C_4 photosynthesis? A modelling analysis. *Journal of Experimental Botany*, 65, 3567-3578.

Wu, A., Hammer, G.L., Doherty, A., von Caemmerer, S., & Farquhar, G.D. (2019). Quantifying impacts of enhancing photosynthesis on crop yield. *Nature Plants*, 5(4), 380-388.

Yamori, W., Sakata, N., Suzuki, Y., Shikanai, T., & Makino, A. (2011). Cyclic electron transport around photosystem I via chloroplast NAD(P)H dehydrogenase (NDH) complex performs a significant physiological role during photosynthesis and plant growth at low temperature in rice. *The Plant Journal*, 68, 966-976.

Yin, X., & Struik, P.C. (2008). Applying modelling experiences from the past to shape crop systems biology: The need to converge crop physiology and functional genomics. *New Phytologist*, 179, 629-642.

Yin, X., & Struik, P.C. (2009). Theoretical reconsiderations when estimating the mesophyll conductance to CO_2 diffusion in leaves of C_3 plants by analysis of combined gas exchange and chlorophyll fluorescence measurements. *Plant, Cell & Environment*, 32, 1513-1524 (with corrigendum in PC&E 33, 1595).

Yin, X., & Struik, P.C. (2012). Mathematical review of the energy transduction stoichiometries of C_4 leaf photosynthesis under limiting light. *Plant, Cell & Environment*, 35, 1299-1312.

Yin, X., & Struik, P.C. (2017a). Can increased leaf photosynthesis be converted into higher crop mass production? A simulation study for rice using the crop model GECROS. *Journal of Experimental Botany*, 68, 2345-2360.

Yin, X., & Struik, P.C. (2017b). Simple generalisation of a mesophyll resistance model for various intracellular arrangements of chloroplasts and mitochondria in C_3 leaves. *Photosynthesis Research*, 132, 211-220.

Yin, X., & Struik, P.C. (2018). The energy budget in C_4 photosynthesis: insights from a cell-type-specific electron transport model. *New Phytologist*, 218, 986-998.

Yin, X., & Struik, P.C. (2021). Exploiting differences in the energy budget among C_4 subtypes to improve crop productivity. *New Phytologist*, 229, 2400-2409.

Yin, X., Harbinson, J., & Struik, P.C. (2006). Mathematical review of literature to assess alternative electron transports and interphotosystem excitation partitioning of steady-state C_3 photosynthesis under limiting light. *Plant, Cell & Environment*, 29, 1771-1782.

Yin, X., Struik, P.C., Romero, P., Harbinson, J., Evers, J.B., van der Putten, P.E.L., & Vos, J. (2009). Using combined measurements of gas exchange and chlorophyll fluorescence to estimate parameters

of a biochemical C_3 photosynthesis model: a critical appraisal and a new integrated approach applied to leaves in a wheat (*Triticum aestivum*) canopy. *Plant, Cell & Environment* 32, 448-464.

Yin, X., Sun, Z., Struik, P.C., van der Putten, P.E.L., van Ieperen, W., & Harbinson, J. (2011). Using a biochemical C_4-photosynthesis model and combined gas exchange and chlorophyll fluorescence measurements to estimate bundle-sheath conductance of maize leaves differing in age and nitrogen content. *Plant, Cell & Environment*, 34, 2183-2199.

Yin, X., van der Putten, P.E.L., Driever, S.M., & Struik, P.C. (2016). Temperature response of bundle-sheath conductance in maize leaves. *Journal of Experimental Botany*, 67, 2699-2714.

Yin, X., van der Putten, P.E.L., Belay, D., & Struik, P.C. (2020). Using photorespiratory oxygen response to analyse leaf mesophyll resistance. *Photosynthesis Research*, 144, 85-99.

Yin, X., van Oijen, M., & Schapendonk, A.H.C.M. (2004). Extension of a biochemical model for the generalized stoichiometry of electron transport limited C_3 photosynthesis. *Plant, Cell & Environment*, 27, 1211-1222.

Zhu, X.-G., Portis Jr., A.R., & Long, S.P. (2004). Would transformation of C_3 crop plants with foreign Rubisco increase productivity? A computational analysis extrapolating from kinetic properties to canopy photosynthesis. *Plant, Cell & Environment*, 27, 155-165.

Table 1 List of used acronyms

Acronym	Definition
BS	Bundle sheath
CCM	CO_2-concentrating mechanism
CET	Cyclic electron transport around Photosystem I
CH_2-THF	5,10-methylene-tetrahydrofolate
FvCB model	The model of Farquhar, von Caemmerer & Berry (1980)
GDC	Glycine decarboxylase
H^+	Proton
IAS	Intercellular air spaces
LET	Linear electron transport (i.e. the noncyclic electron transport for supporting the Calvin-Benson cycle and the photorespiratory cycle)
M	Mesophyll
NAD-ME	Nicotinamide adenine dinucleotide-malic enzyme
NADP-ME	Nicotinamide adenine dinucleotide phosphate-malic enzyme
NDH	NAD(P)H dehydrogenase
PEP	Phospho*enol*pyruvate
PEPc	Phospho*enol*pyruvate carboxylase
PEP-CK	Phospho*enol*pyruvate-carboxykinase
3-PGA	3-phosphoglycerate
P_i	Phosphate
PPDK	Pyruvate phosphate dikinase
PSI	Photosystem I
PSII	Photosystem II
RuBP	Ribulose 1,5-bisphosphate
THF	Tetrahydrofolate
TP	Triose phosphate
TPU	Triose phosphate utilisation

Table 2 List of model symbols

Symbol	Definition	Unit
a	Fraction of oxaloacetate that is reduced in mesophyll cells to malate moving to drive bundle sheath mitochondrial electron transport to produce ATP	-
A	Rate of CO_2 assimilation	μmol m^{-2} s^{-1}
A_c	Rate of CO_2 assimilation limited by Rubisco activity	μmol m^{-2} s^{-1}
A_j	Rate of CO_2 assimilation limited by electron transport	μmol m^{-2} s^{-1}
A_p	Rate of CO_2 assimilation limited by triose phosphate utilisation	μmol m^{-2} s^{-1}
C_c	CO_2 partial pressure at the carboxylating sites of Rubisco	μbar
C_i	CO_2 partial pressure at intercellular-air spaces	μbar
C_m	CO_2 partial pressure at mesophyll cytosol	μbar
f	Fraction of irradiance absorbed by photosynthetic pigments but unavailable for Calvin-Benson and photorespiratory cycles	-
F	Rate of photorespiratory CO_2 release	μmol m^{-2} s^{-1}
f_{cyc}	Fraction of Photosystem I electrons that follow cyclic electron transport	-
f_{NDH}	Fraction of cyclic electron transport that follow the NAD(P)H dehydrogenase-dependent pathway	-
f_{pseudo}	Fraction of the Photosystem I electrons that follow the pseudocyclic electron transport	-
f_{refix}	Fraction of respired and photorespired CO_2 that is refixed	-
$f_{refix,cell}$	Fraction of respired and photorespired CO_2 that is refixed within mesophyll cells	-
$f_{refix,ias}$	Fraction of respired and photorespired CO_2 that is refixed via the intercellular air spaces	-
f_Q	Fraction of electrons at plastoquinone that follow the Q cycle	-
g_{bs}	Bundle-sheath conductance	mol m^{-2} s^{-1} bar^{-1}
g_m	Mesophyll conductance (inverse of mesophyll resistance)	mol m^{-2} s^{-1} bar^{-1}
g_{mo}	Mesophyll conductance constant, applied to the constant mesophyll conductance mode	mol m^{-2} s^{-1} bar^{-1}
h	Protons required per ATP synthesis (i.e. the H^+:ATP ratio)	mol mol^{-1}
I_{abs}	Irradiance absorbed by photosynthetic pigments	μmol m^{-2} s^{-1}
J	Potential electron transport rate	μmol m^{-2} s^{-1}
J_1	Potential electron transport rate through Photosystem I	μmol m^{-2} s^{-1}
J_2	Potential electron transport rate through Photosystem II	μmol m^{-2} s^{-1}
J_{atp}	Potential rate of chloroplastic ATP production	μmol m^{-2} s^{-1}
J_{max}	Light-saturated potential electron transport rate	μmol m^{-2} s^{-1}
J_{2max}	Light-saturated potential electron transport rate through Photosystem II	μmol m^{-2} s^{-1}
k	Factor allowing for the effect of chloroplast gaps and the cytosol resistance such that the term $k\lambda$ defines as the fraction of (photo)respiratory CO_2 in the inner cytosol ($0 \leq k\lambda \leq 1$)	-
K_{mC}	Michaelis-Menten constant of Rubisco for CO_2	μbar
K_{mO}	Michaelis-Menten constant of Rubisco for O_2	mbar
K_p	Michaelis-Menten constant of PEPc for CO_2	μbar
L	Rate of CO_2 leakage from bundle-sheath to mesophyll cells	μmol m^{-2} s^{-1}
m	Parameter lumping several mesophyll properties, $= (1-\lambda k)r_{ch}/r_m$ with $0 \leq m \leq 1$	-
n	ATP produced per NADH oxidation	mol mol^{-1}
O_c	O_2 partial pressure at the active sites of Rubisco	mbar
O_m	O_2 partial pressure at mesophyll cytosol	mbar
r_{ch}	Chloroplast envelope and stroma resistance	mol^{-1} m^2 s bar

r_{cx}	Carboxylation resistance	mol^{-1} m^2 s bar
r_m	Mesophyll resistance	mol^{-1} m^2 s bar
r_{sc}	Stomatal resistance to CO_2 transfer	mol^{-1} m^2 s bar
r_{wp}	Cell-wall and plasma-membrane resistance	mol^{-1} m^2 s bar
$S_{c/o}$	Relative CO_2/O_2 specificity of Rubisco	mbar μbar^{-1}
T_p	Rate of triose phosphate utilisation	μmol m^{-2} s^{-1}
u_{oc}	Coefficient that lumps diffusivities of O_2 and CO_2 in water and their respective Henry constants, = 0.047 at 25°C	μmol μbar (μmol mbar)$^{-1}$
V_c	RuBP carboxylation rate	μmol m^{-2} s^{-1}
V_{cmax}	CO_2-saturated maximum carboxylation rate of Rubisco	μmol m^{-2} s^{-1}
V_o	RuBP oxygenation rate	μmol m^{-2} s^{-1}
V_p	PEP carboxylation rate	μmol m^{-2} s^{-1}
V_{pmax}	Maximum carboxylation rate of PEPc	μmol m^{-2} s^{-1}
R_d	Day respiration (CO_2 release in the light by processes other than photorespiration)	μmol m^{-2} s^{-1}
R_m	Day respiration in the mesophyll cells	μmol m^{-2} s^{-1}
W_c	RuBP carboxylation rate limited by Rubisco activity	μmol m^{-2} s^{-1}
W_j	RuBP carboxylation rate limited by electron transport	μmol m^{-2} s^{-1}
W_p	RuBP carboxylation rate limited by triose phosphate utilisation	μmol m^{-2} s^{-1}
x	Fraction of the chloroplastic ATP that is used for the CO_2-Concentrating Mechanism cycle	-
z	Factor for ATP production per Photosystem II electron when the cyclic electron transport runs simultaneously	mol mol^{-1}
α	Fraction of glycolate carbon not returned to chloroplast	-
$\alpha_{2(LL)}$	Quantum yield of Photosystem II electron transport (under limiting light) on the basis of light absorbed by both photosystems	mol mol^{-1}
α_{bs}	Fraction of Photosystem II that is in the bundle-sheath cells	-
α_G	Fraction of glycolate carbon taken out from the photorespiratory pathway as glycine	-
α_S	Fraction of glycolate carbon taken out from the photorespiratory pathway as serine	-
α_T	Fraction of glycolate carbon taken out from the photorespiratory pathway as CH_2-THF	-
δ	Factor defining a variable mesophyll conductance mode	-
ϕ	RuBP oxygenation : RuBP carboxylation ratio, = V_o:V_c	-
ϕ_L	Leakiness, = L/V_p	-
$\Phi_{1(LL)}$	Quantum yield of Photosystem I electron transport (under limiting light)	mol mol^{-1}
$\Phi_{2(LL)}$	Quantum yield of Photosystem II electron transport (under limiting light)	mol mol^{-1}
$\Phi_{CO2(LL)}$	Quantum yield of CO_2 uptake (under limiting light)	mol mol^{-1}
$\Phi_{O2(LL)}$	Quantum yield of O_2 evolution (under limiting light)	mol mol^{-1}
φ	Chloroplastic ATP required per C_4 cycle, = 2 for the NADP-ME and NAD-ME subtypes and = 2–(n+1)a for the PEP-CK subtype	mol ATP (mol CO_2)$^{-1}$
γ_*	Half the inverse of Rubisco specificity, = $0.5/S_{c/o}$	μbar mbar^{-1}
Γ_*	CO_2-compensation point in the absence of day respiration, = $0.5O_c/S_{c/o}$	μbar
Γ_{*GT}	Modified Γ_* as a result of glycolate carbon exit in the form of glycine and CH_2-THF from the photorespiratory pathway, = $(1-\alpha_G+2\alpha_T)\Gamma_*$	μbar
λ	Fraction of mitochondria that locate closely behind chloroplasts in the inner cytosol	-
θ	Curvature factor of light response of electron transport	-
ρ_2	Factor for excitation partitioning to Photosystem II, = $\alpha_{2(LL)}/\Phi_{2(LL)}$	-

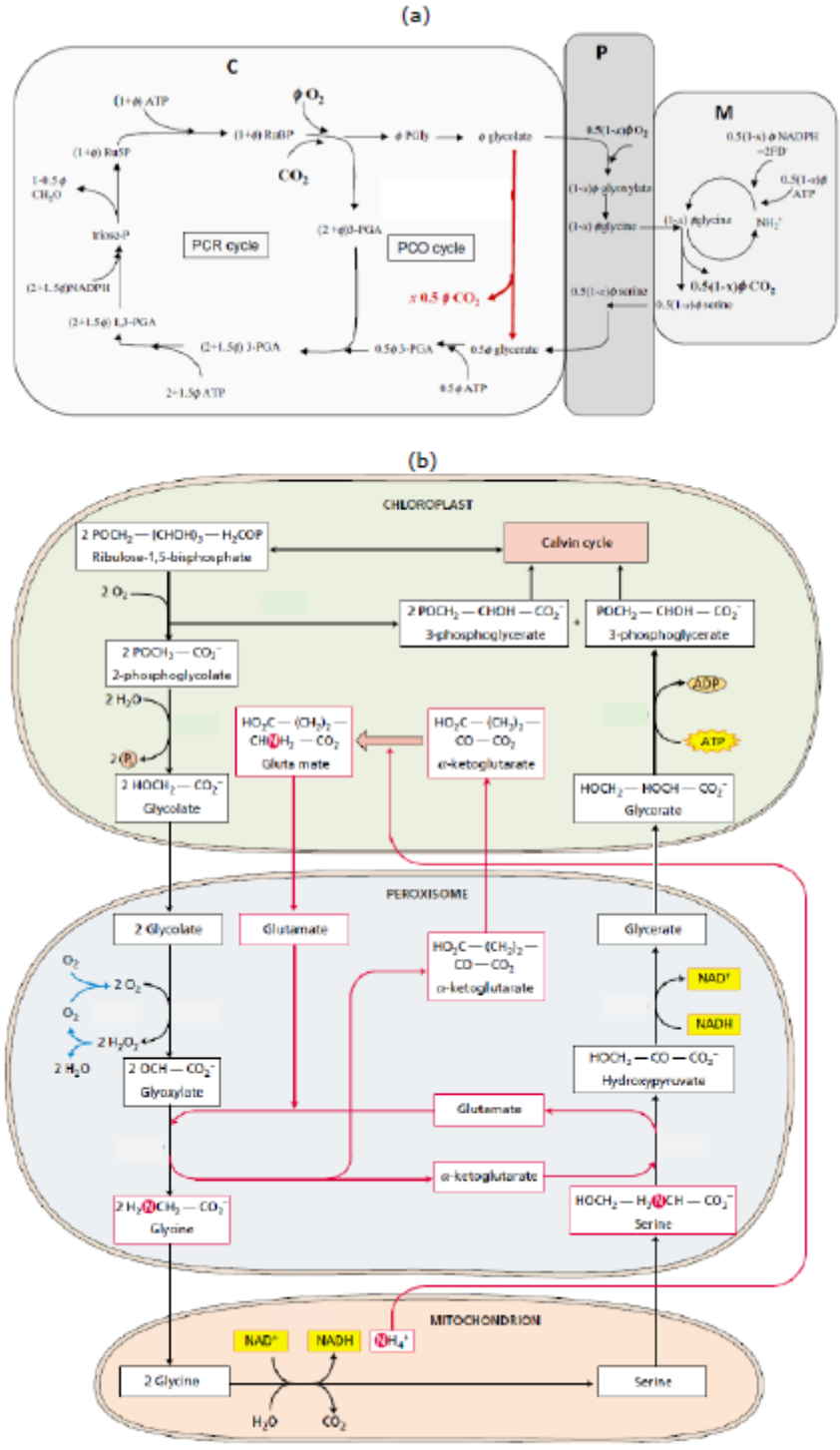

Fig. 1 The stoichiometry of the Calvin-Benson cycle or photosynthetic carbon reduction (PCR) cycle and the photorespiratory carbon oxidation (PCO) cycle. Panel (a) is redrawn from von Caemmerer (2013), where ϕ denotes the oxygenation to carboxylation ratio. The complete photorespiratory cycle involves the chloroplast (C), the peroxisome (P), and the mitochondrion (M) where CO_2 from glycine decarboxylation is released. The red line indicates the so-called photorespiratory bypass, enabling a fraction (x) of the photorespiratory CO_2 released in the chloroplast, which not only increases the chance for the photorespiratory CO_2 being refixed by Rubisco in chloroplast, but may also decrease the energy (ATP and reduced ferredoxin) requirement associated with the recycling of ammonia released from glycine decarboxylation. No attempt is made here to calculate the exact change of energy requirement, because that depends on the type of bypass (Peterhansel et al. 2013). Abbreviations: 3-PGA: 3-phosphoglycerate; 1,3-PGA: 1,3-bisphosphoglycerate; FD, reduced ferredoxin; PGly, phosphoglycolate; Ru5P: ribulose 5-phosphate; RuBP: ribulose 1,5-bisphosphate; triose-P: triose phosphate. Panel (b) shows detailed reactions, and the carbon- and nitrogen-atoms in the metabolites, of the standard photorespiratory cycle (redrawn from Taiz & Zeiger (2002), where the flow of carbon and nitrogen are indicated in black and pink, respectively.

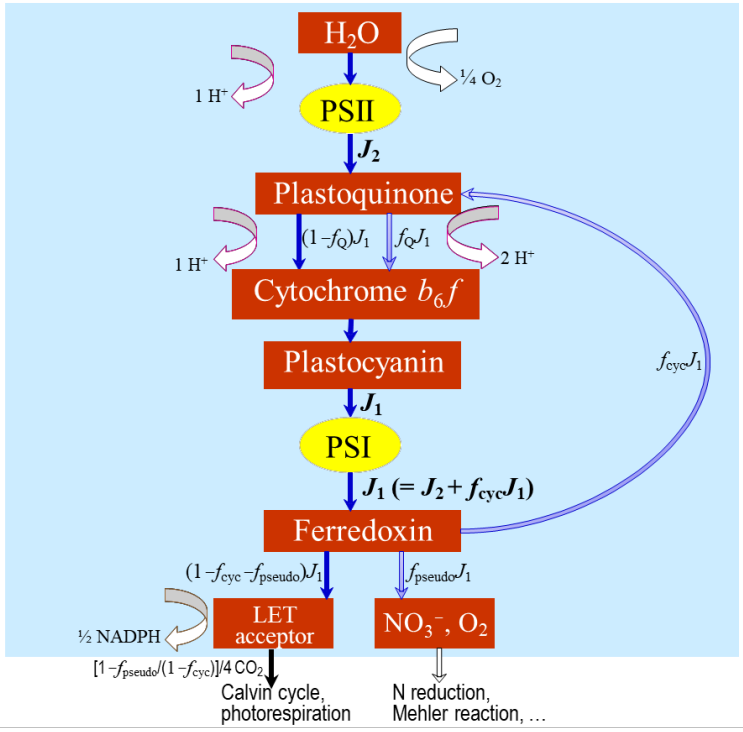

Fig. 2 The scheme for pathways of linear, cyclic and pseudocyclic electron transport (blue arrows) as driven by light energy allocated to Photosystem II (PSII) and Photosystem I (PSI), in the light reactions (with light-blue background) of photosynthesis (revised from Yin et al. 2004). Thick-curved arrows show O_2 evolved, protons (H^+) pumped or NADPH produced per electron transferred. H^+ are required for ATP synthesis, and produced ATP and NADPH (or reductant equivalents) are used for various metabolic processes specified underneath in black phrases. The cyclic electron transport, the pseudocyclic electron transport, and the Q cycle introduced in Extension 2 are shown in thin double-lined arrows and their fluxes are all expressed in proportion to the total electron flux passing PSI (J_1) as $f_{cyc}J_1$, $f_{pseudo}J_1$ and f_QJ_1, respectively. The linear electron transport (LET) as the only pathway defined in the canonical model is shown in thick single-lined arrows and expressed as $(1–f_{cyc}–f_{pseudo})J_1$. In the presence of the cyclic electron transport, the electron flux passing PSII (J_2) is smaller than that passing PSI: $J_2 = (1–f_{cyc})J_1$, instead of $J_2 = J_1$ as implied in the canonical model. In the presence of pseudocyclic electron transport for supporting processes like nitrate reduction, CO_2 uptake is not in a 1:1 ratio to O_2 evolution, but is $[1–f_{pseudo}/(1–f_{cyc})]$ mol CO_2 per mol O_2 evolved (assuming no Mehler reaction), which is the basis for eqn 13b (see the text).

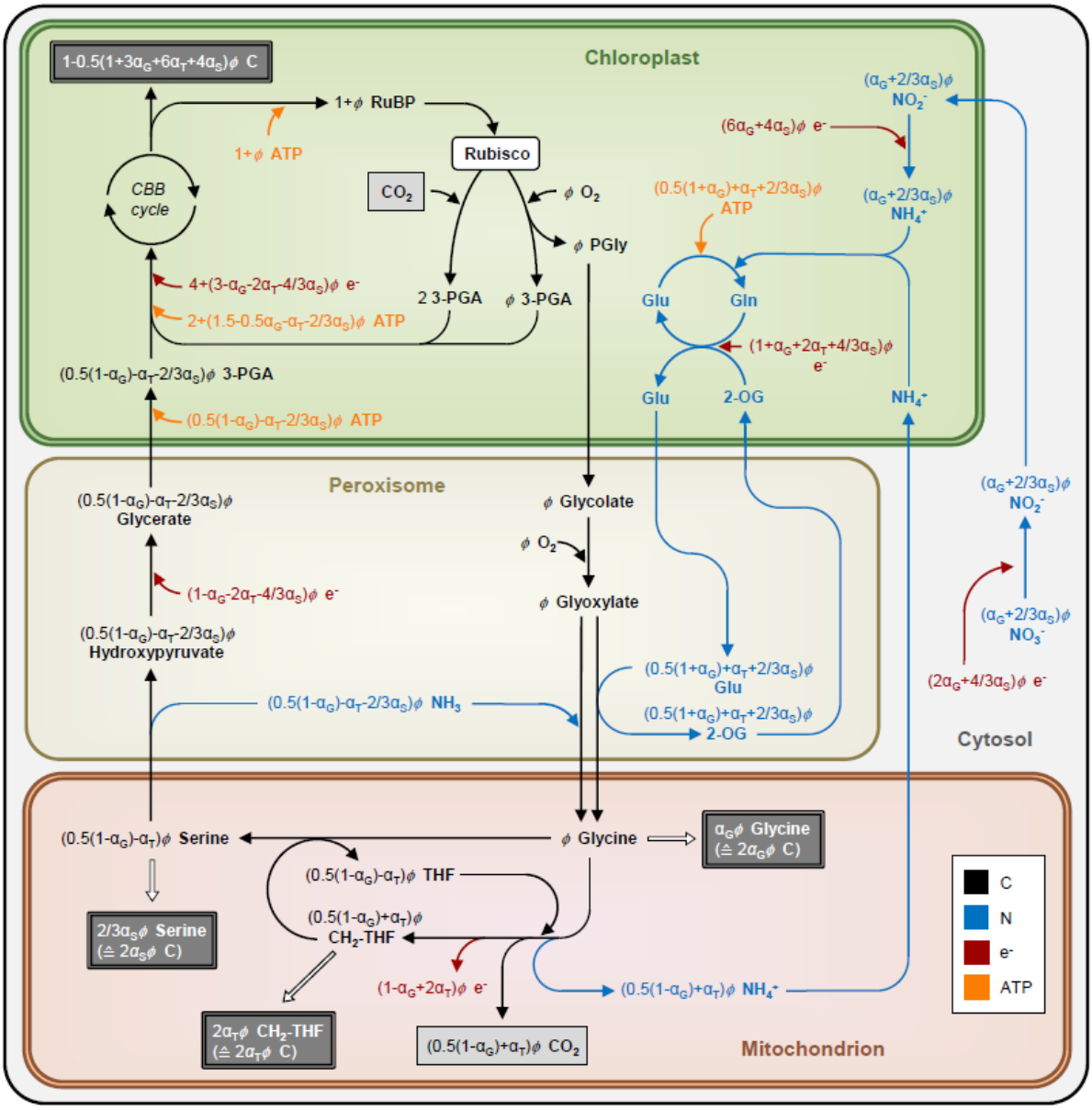

Fig. 3 Stoichiometries of electron (red) and ATP (orange) requirements for the Calvin-Benson-Bassham (CBB) cycle, and for the photorespiratory pathway where there are fractions of glycolate carbon that exits in the form of either glycine (α_G), or CH_2-THF (α_T), or serine (α_S). The RuBP oxygenation to RuBP carboxylation ratio is denoted as ϕ. All these fluxes, also including carbon (in black) and nitrogen (in blue), are scaled in relation to the rate of RuBP carboxylation. The difference between CO_2 taken up by carboxylation and CO_2 released from photorespiration, shown in light grey boxes, equals the sum of individual sinks for assimilated carbon indicated by double-bordered grey boxes (redrawn from Busch 2020). The amount of NO_3^- entering the leaf via *de novo* nitrogen assimilation equals the total flux of nitrogen leaving the pathway in the form of glycine and serine ($\alpha_G+2/3\alpha_S)\phi$. The stoichiometric coefficients for nitrogen assimilation are formulated from the understanding that (i) one mol nitrogen assimilation from nitrate (NO_3^-) into glutamate requires 10 mol electrons, including one mol NADH (equivalent to two electrons) for reducing NO_3^- to nitrite (NO_2^-), six electrons in the form of reduced ferredoxin for reducing NO_2^- to ammonia (NH_4^+), and two electrons again in the form of reduced ferredoxin for the glutamate synthesis from glutamine, and (ii) the formation step of one mol glutamine from NH_4^+ and glutamate also requires one mol ATP, which is the only ATP required for the whole process of NO_3^- reduction (Noctor & Foyer 1998). Note that NADH released from the glycine decarboxylation in the mitochondrion, NADH used for transforming hydroxypyruvate into glycerate in the peroxisome, and NADH used for reducing NO_3^- to NO_2^- in the cytosol are all shown in the electron equivalents. Abbreviations: 2-OG, 2-oxoglutarate; 3-PGA, 3-phosphoglycerate; CH_2-THF, 5,10-methylene-tetrahydrofolate; Gln, glutamine; Glu, glutamate; PGly, phosphoglycolate; RuBP, ribulose 1,5-bisphosphate; THF, tetrahydrofolate.

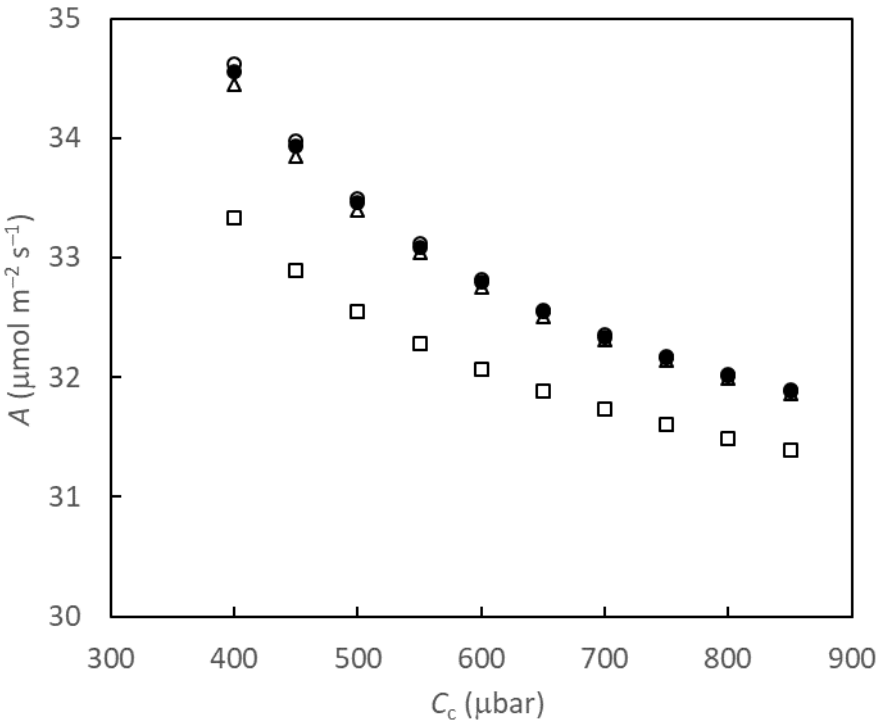

Fig. 4 A-C_c curves within the range of TPU limitation, generated by eqn 16e (with α_T assumed to be zero) assuming both glycine and serine exit with $\alpha_G = 0.1$ and $\alpha_S = 0.2$ (filled circles), by eqn 17a assuming only glycine exit with $\alpha_G = 0.3$ (open triangles), by eqn 17b assuming only serine exit with $\alpha_S = 0.3$ (open circles; but note that "open circles" are largely invisible because most of them overlap "filled circles"), and by eqn 7b with $\alpha = 0.3$ (open squares). Other parameter values for this illustration: $T_p = 10$ μmol m^{-2} s^{-1}, $\Gamma_* = 40$ μbar, and $R_d = 0$ μmol m^{-2} s^{-1}. Not shown is that if the model eqn 17a or eqn 17b is used to fit the curve of the filled circles, the obtained α_G or α_S was 0.305 or 0.298, respectively (both still *ca* 0.3) while maintaining T_p the same. If eqn 7b is used to fit the curve of the filled circles, the obtained α was 0.397 with the same T_p, suggesting eqn 7b over-estimates the fraction of glycolate carbon not returned to the chloroplast by a factor of 4/3, which is due to not accounting for that exported glycine does not contribute to the 1 in 4 carbons lost by photorespiration.

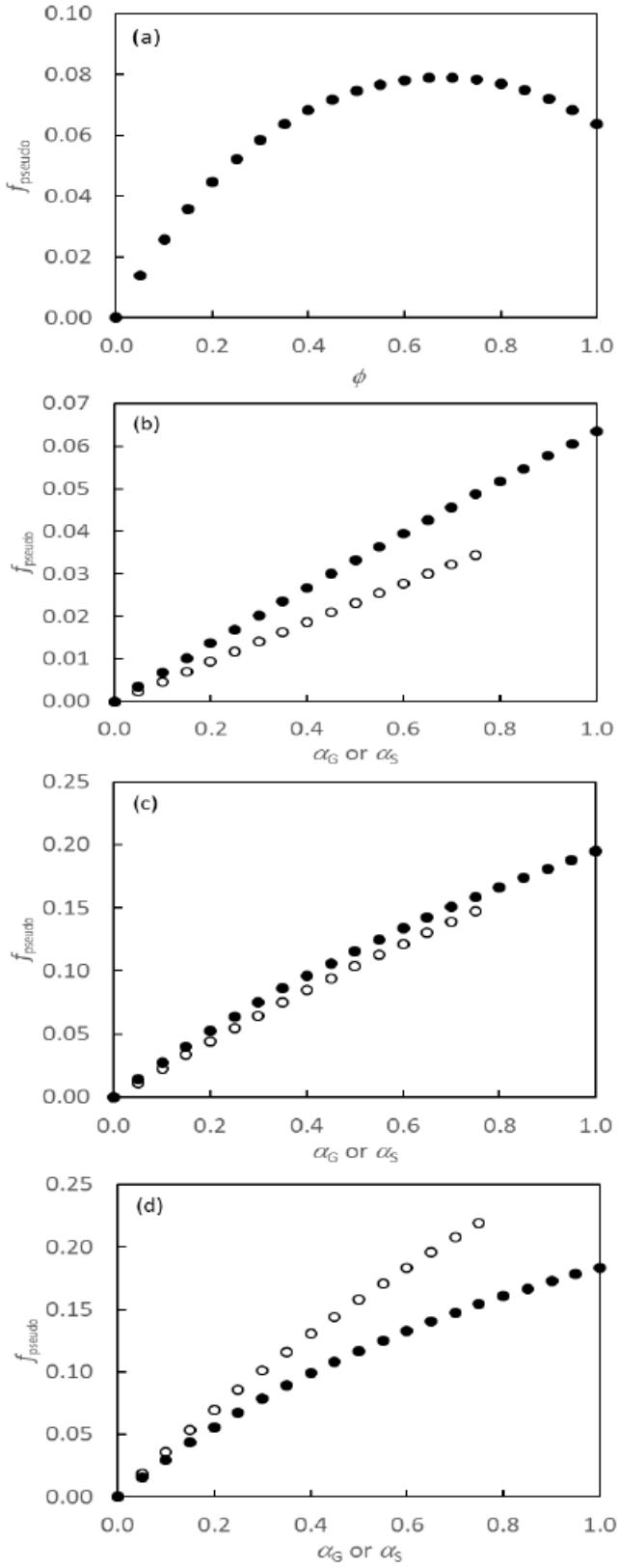

Fig. 5 The eqn 18b calculated fraction of the total PSI electron flux as pseudocyclic electron transport (f_{pseudo}) for supporting nitrogen assimilation associated with the photorespiratory pathway (assuming a negligible cyclic electron transport), (a) as a function of the oxygenation to carboxylation ratio ϕ when α_G (fraction of glycolate carbon leaving the pathway as glycine) = 0.1 and α_S (fraction of glycolate carbon leaving the pathway as serine) = 0.15, and (b, c, d) as a function of α_G when α_S is set to 0 (filled symbols) or of α_S when α_G is set to 0 (open symbols) when ϕ is fixed at 0.05, 0.30 and 0.60, respectively.

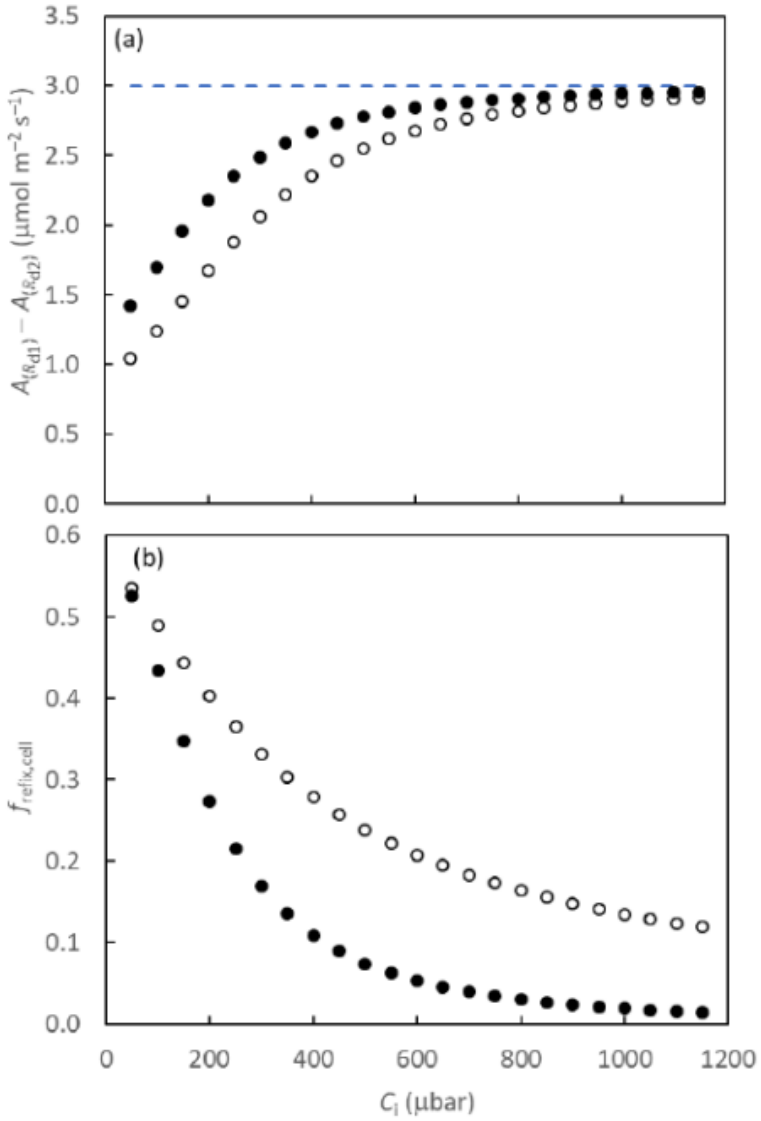

Fig. 6 (a) The calculated difference in net photosynthesis A, using the coupled g_m-FvCB model, eqn 20, for two hypothetical leaves whose day respiration (R_d) is preset as 0 μmol m^{-2} s^{-1} (R_{d1}) and 3 μmol m^{-2} s^{-1} (R_{d2}), respectively, - the difference in R_d as indicated by the horizontal line. The calculation used the algorithm assuming an electron transport limitation for the simplest situation of eqn 20, i.e. $\alpha_G = \alpha_S = \alpha_T = 0$, $m = 0$, $\delta = 0$ (for the constant g_m scenario). The values used for g_m were 0.25 (filled symbols) or 0.15 (open symbols) mol m^{-2} s^{-1} bar^{-1}. (b) The calculated fractions of refixation within the mesophyll cell ($f_{refix,cell}$) using eqn 21b without the term r_{sc} (open symbols) or using the formula that $f_{refix,cell} = 1 - [A_{(Rd1)} - A_{(Rd2)}]/(R_{d2} - R_{d1})$ (filled symbols). The calculation in (b) assumed that $g_m = 0.25$ mol m^{-2} s^{-1} bar^{-1}. Other parameter values used for both panels (a) and (b): $J = 150$ μmol m^{-2} s^{-1}, and $\Gamma^* = 40$ μbar.

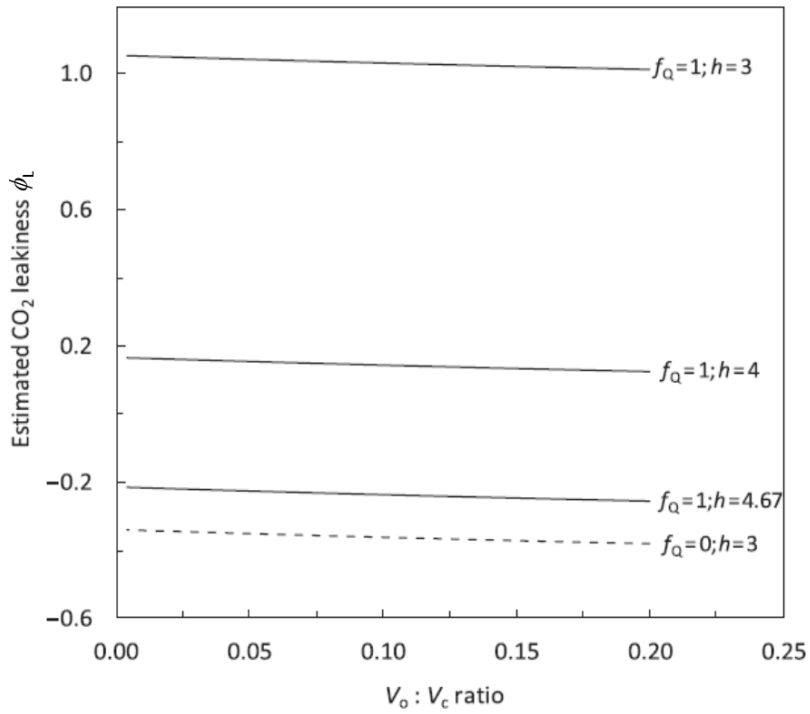

Fig. 7 The CO_2 leakiness ϕ_L calculated by eqn 23b as a function of oxygenation to carboxylation ratio (V_o:V_c), using different values for the H^+:ATP ratio (h) combined either with or without the Q cycle (f_Q). The results without the Q cycle ($f_Q = 0$) combined with $h = 4$ or 4.67 are not shown because these combinations gave very negative estimates of leakiness (redrawn from Yin & Struik 2012). The scenario for possible involvement of the NAD(P)H dehydrogenase-dependent pathway (f_{NDH}) in the cyclic electron transport is not given in this figure, but see the discussion in the text.